Molecular reaction dynamics

24

The simplest quantitative account of reaction rates is in terms of collision theory, which can be used only for the discussion of reactions between simple species in the gas phase. Reactions in solution are classified into two types: diffusion-controlled and activation-controlled. The former can be expressed quantitatively in terms of the diffusion equation. In transition state theory, it is assumed that the reactant molecules form a complex that can be discussed in terms of the population of its energy levels. Transition state theory inspires a thermodynamic approach to reaction rates, in which the rate constant is expressed in terms of thermodynamic parameters. This approach is useful for parametrizing the rates of reactions in solution. The highest level of sophistication is in terms of potential energy surfaces and the motion of molecules through these surfaces. As we shall see, such an approach gives an intimate picture of the events that occur when reactions occur and is open to experimental study. We also use transition state theory to examine the transfer of electrons in homogeneous systems and see that the rate of the process depends on the distance between electron donor and acceptor, the standard Gibbs energy of reaction, and the energy associated with molecular rearrangements that accompany the transfer of charge.

Now we are at the heart of chemistry. Here we examine the details of what happens to molecules at the climax of reactions. Extensive changes of structure are taking place and energies the size of dissociation energies are being redistributed among bonds: old bonds are being ripped apart and new bonds are being formed.

As may be imagined, the calculation of the rates of such processes from first principles is very difficult. Nevertheless, like so many intricate problems, the broad features can be established quite simply. Only when we enquire more deeply do the complications emerge. In this chapter we look at several approaches to the calculation of a rate constant for elementary bimolecular processes, ranging from electron transfer to chemical reactions involving bond breakage and formation. Although a great deal of information can be obtained from gas-phase reactions, many reactions of interest take place in solution, and we shall also see to what extent their rates can be predicted.

Reactive encounters

In this section we consider two elementary approaches to the calculation of reaction rates, one relating to gas-phase reactions and the other to reactions in solution. Both approaches are based on the view that reactant molecules must meet, and that reaction takes place only if the molecules have a certain minimum energy. In the collision theory of bimolecular gas-phase reactions, which we mentioned briefly in Section 22.5,

products are formed only if the collision is sufficiently energetic; otherwise the colliding reactant molecules separate again. In solution, the reactant molecules may simply diffuse together and then acquire energy from their immediate surroundings while they are in contact.

24.1 Collision theory

We shall consider the bimolecular elementary reaction

$$A + B \rightarrow P \qquad v = k_2[A][B] \tag{24.1}$$

where P denotes products, and aim to calculate the second-order rate constant k_2.

We can anticipate the general form of the expression for k_2 by considering the physical requirements for reaction. We expect the rate v to be proportional to the rate of collisions, and therefore to the mean speed of the molecules, $\bar{c} \propto (T/M)^{1/2}$ where M is the molar mass of the molecules, their collision cross-section, σ, and the number densities $\mathcal{N}_A$ and $\mathcal{N}_B$ of A and B:

$$v \propto \sigma(T/M)^{1/2}\mathcal{N}_A\mathcal{N}_B \propto \sigma(T/M)^{1/2}[A][B]$$

However, a collision will be successful only if the kinetic energy exceeds a minimum value, the activation energy, E_a, of the reaction. This requirement suggests that the rate constant should also be proportional to a Boltzmann factor of the form $e^{-E_a/RT}$. So we can anticipate, by writing the reaction rate in the form given in eqn 24.1, that

$$k_2 \propto \sigma(T/M)^{1/2}e^{-E_a/RT}$$

Not every collision will lead to reaction even if the energy requirement is satisfied, because the reactants may need to collide in a certain relative orientation. This 'steric requirement' suggests that a further factor, P, should be introduced, and that

$$k_2 \propto P\sigma(T/M)^{1/2}e^{-E_a/RT} \tag{24.2}$$

As we shall see in detail below, this expression has the form predicted by collision theory. It reflects three aspects of a successful collision:

$$k_2 \propto \text{steric requirement} \times \text{encounter rate} \times \text{minimum energy requirement}$$

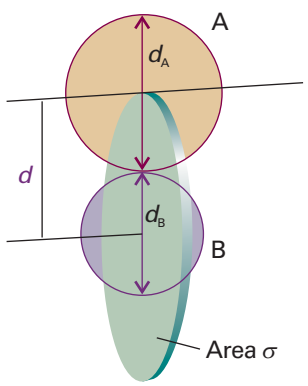

Fig. 24.1 The collision cross-section for two molecules can be regarded to be the area within which the projectile molecule (A) must enter around the target molecule (B) in order for a collision to occur. If the diameters of the two molecules are d_A and d_B, the radius of the target area is $d = \frac{1}{2}(d_A + d_B)$ and the cross-section is πd^2.

(a) Collision rates in gases

We have anticipated that the reaction rate, and hence k_2, depends on the frequency with which molecules collide. The **collision density**, Z_{AB}, is the number of (A,B) collisions in a region of the sample in an interval of time divided by the volume of the region and the duration of the interval. The frequency of collisions of a single molecule in a gas was calculated in Section 21.1. As shown in the *Justification* below, that result can be adapted to deduce that

$$Z_{AB} = \sigma\left(\frac{8kT}{\pi\mu}\right)^{1/2} N_A^2[A][B] \tag{24.3a}$$

where σ is the collision cross-section (Fig. 24.1)

$$\sigma = \pi d^2 \qquad d = \tfrac{1}{2}(d_A + d_B) \tag{24.3b}$$

and μ is the reduced mass,

$$\mu = \frac{m_A m_B}{m_A + m_B} \tag{24.3c}$$

Similarly, the collision density for like molecules at a molar concentration [A] is

$$Z_{AA} = \sigma\left(\frac{4kT}{\pi m_A}\right)^{1/2} N_A^2[A]^2 \tag{24.4}$$

Collision densities may be very large. For example, in nitrogen at room temperature and pressure, with $d = 280$ pm, $Z = 5 \times 10^{34}$ m^{-3} s^{-1}.

Justification 24.1 *The collision density*

It follows from eqn 21.11 that the collision frequency, z, for a single A molecule of mass m_A in a gas of other A molecules is

$$z = \sigma \bar{c}_{rel} \mathcal{N}_A \tag{24.5}$$

where $\mathcal{N}_A$ is the number density of A molecules and $\bar{c}_{rel}$ is their relative mean speed. As indicated in Section 21.1a,

$$\bar{c}_{rel} = 2^{1/2}\bar{c} \qquad \bar{c} = \left(\frac{8kT}{\pi m}\right)^{1/2} \tag{24.6}$$

For future convenience, it is sensible to introduce $\mu = \frac{1}{2}m$ (for like molecules of mass m), and then to write

$$\bar{c}_{rel} = \left(\frac{8kT}{\pi\mu}\right)^{1/2} \tag{24.7}$$

This expression also applies to the mean relative speed of dissimilar molecules, provided that μ is interpreted as the reduced mass in eqn 24.5.

The total collision density is the collision frequency multiplied by the number density of A molecules:

$$Z_{AA} = \tfrac{1}{2} z \mathcal{N}_A = \tfrac{1}{2}\sigma \bar{c}_{rel} \mathcal{N}_A^2 \tag{24.8}$$

The factor of $\frac{1}{2}$ has been introduced to avoid double counting of the collisions (so one A molecule colliding with another A molecule is counted as one collision regardless of their actual identities). For collisions of A and B molecules present at number densities $\mathcal{N}_A$ and $\mathcal{N}_B$, the collision density is

$$Z_{AB} = \sigma \bar{c}_{rel} \mathcal{N}_A \mathcal{N}_B \tag{24.9}$$

Note that we have discarded the factor of $\frac{1}{2}$ because now we are considering an A molecule colliding with any of the B molecules as a collision.

The number density of a species J is $\mathcal{N}_J = N_A[J]$, where [J] is their molar concentration and N_A is Avogadro's constant. Equations 24.3 and 24.4 then follow.

(b) The energy requirement

According to collision theory, the rate of change in the molar concentration of A molecules is the product of the collision density and the probability that a collision occurs with sufficient energy. The latter condition can be incorporated by writing the collision cross-section as a function of the kinetic energy of approach of the two colliding species, and setting the cross-section, $\sigma(\varepsilon)$, equal to zero if the kinetic energy of approach is below a certain threshold value, ε_a. Later, we shall identify $N_A\varepsilon_a$ as E_a, the (molar) activation energy of the reaction. Then, for a collision with a specific relative speed of approach v_{rel} (not, at this stage, a mean value),

$$\frac{d[A]}{dt} = -\sigma(\varepsilon) v_{rel} N_A [A][B] \tag{24.10}$$

Comment 24.1

See *Further information* 10.1. The kinetic energy associated with the relative motion of two particles takes the form $\varepsilon = \frac{1}{2}\mu v_{rel}^2$ when the centre-of-mass coordinates are separated from the internal coordinates of each particle.

Comment 24.2

To go from eqn 24.10 to eqn 24.11, we need to review concepts of probability theory summarized in *Appendix* 2. Namely, the mean value of a continuous variable X is given by

$$\langle X\rangle = \int x f(x)\,\mathrm{d}x$$

where the integral is over all values x that X can assume and the probability of finding a value of X between x and $x + \mathrm{d}x$ is $f(x)\mathrm{d}x$, with $f(x)$ a measure of the distribution of the probability values over x. The mean value of a function $g(X)$ is given by

$$\langle g(X)\rangle = \int g(x) f(x)\,\mathrm{d}x$$

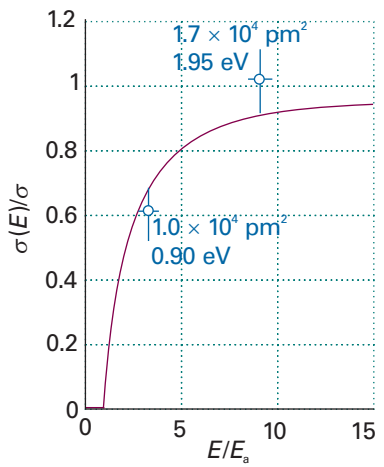

Fig. 24.2 The variation of the reactive cross-section with energy as expressed by eqn 24.13. The data points are from experiments on the reaction $H + D_2 \rightarrow HD + D$ (K. Tsukiyama, B. Katz, and R. Bersohn, *J. Chem. Phys.* **84**, 1934 (1986)).

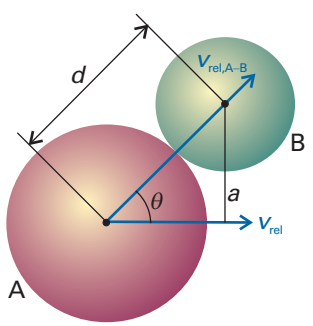

Fig. 24.3 The parameters used in the calculation of the dependence of the collision cross-section on the relative kinetic energy of two molecules A and B.

The relative kinetic energy, ε, and the relative speed are related by $\varepsilon = \frac{1}{2}\mu v_{\mathrm{rel}}^2$, so $v_{\mathrm{rel}} = (2\varepsilon/\mu)^{1/2}$. At this point we recognize that a wide range of approach energies is present in a sample, so we should average the expression just derived over a Boltzmann distribution of energies $f(\varepsilon)$, and write (see *Comment* 24.2)

$$\frac{\mathrm{d[A]}}{\mathrm{d}t} = -\left\{\int_0^\infty \sigma(\varepsilon) v_{\mathrm{rel}} f(\varepsilon)\,\mathrm{d}\varepsilon\right\} N_{\mathrm{A}}[\mathrm{A}][\mathrm{B}] \tag{24.11}$$

and hence recognize the rate constant as

$$k_2 = N_{\mathrm{A}} \int_0^\infty \sigma(\varepsilon) v_{\mathrm{rel}} f(\varepsilon)\,\mathrm{d}\varepsilon \tag{24.12}$$

Now suppose that the reactive collision cross-section is zero below ε_{a}. We show in the *Justification* below that, above ε_{a}, $\sigma(\varepsilon)$ varies as

$$\sigma(\varepsilon) = \left(1 - \frac{\varepsilon_{\mathrm{a}}}{\varepsilon}\right)\sigma \tag{24.13}$$

This form of the energy dependence is broadly consistent with experimental determinations of the reaction between H and D_2 as determined by molecular beam measurements of the kind described later (Fig. 24.2). Then, in the *Justification* below, we show that

$$k_2 = N_{\mathrm{A}} \sigma \bar{c}_{\mathrm{rel}} \mathrm{e}^{-E_{\mathrm{a}}/RT} \tag{24.14}$$

Justification 24.2 *The rate constant*

Consider two colliding molecules A and B with relative speed v_{rel} and relative kinetic energy $\varepsilon = \frac{1}{2}\mu v_{\mathrm{rel}}^2$ (Fig. 24.3). Intuitively we expect that a head-on collision between A and B will be most effective in bringing about a chemical reaction. Therefore, $v_{\mathrm{rel,A–B}}$, the magnitude of the relative velocity component parallel to an axis that contains the vector connecting the centres of A and B, must be large. From trigonometry and the definitions of the distances a and d, and the angle θ given in Fig. 24.3, it follows that

$$v_{\mathrm{rel,A–B}} = v_{\mathrm{rel}} \cos\theta = v_{\mathrm{rel}} \left(\frac{d^2 - a^2}{d^2}\right)^{1/2} \tag{24.15}$$

We assume that only the kinetic energy associated with the head-on component of the collision, $\varepsilon_{\mathrm{A–B}}$, can lead to a chemical reaction. After squaring both sides of the equation above and multiplying by $\frac{1}{2}\mu$, it follows that

$$\varepsilon_{\mathrm{A–B}} = \varepsilon \frac{d^2 - a^2}{d^2} \tag{24.16}$$

The existence of an energy threshold, ε_{a}, for the formation of products implies that there is a maximum value of a, a_{max}, above which reactions do not occur. Setting $a = a_{\mathrm{max}}$ and $\varepsilon_{\mathrm{A–B}} = \varepsilon_{\mathrm{a}}$ in the equation above gives

$$a_{\mathrm{max}}^2 = \left(1 - \frac{\varepsilon_{\mathrm{a}}}{\varepsilon}\right) d^2 \tag{24.17}$$

Substitution of $\sigma(\varepsilon)$ for πa_{max}^2 and σ for πd^2 in the equation above gives eqn 24.13. Note that the equation can be used only when $\varepsilon > \varepsilon_{\mathrm{a}}$.

We proceed with the calculation of the rate constant by considering the Maxwell–Boltzmann distribution of molecular speeds given in Section 21.1. It may be expressed

in terms of the kinetic energy, ε, by writing $\varepsilon = \frac{1}{2}\mu v^2$, then $\mathrm{d}v = \mathrm{d}\varepsilon/(2\mu\varepsilon)^{1/2}$ and eqn 21.4 becomes

$$f(v)\mathrm{d}v = 4\pi\left(\frac{\mu}{2\pi kT}\right)^{3/2}\left(\frac{2\varepsilon}{\mu}\right)\mathrm{e}^{-\varepsilon/kT}\frac{\mathrm{d}\varepsilon}{(2\mu\varepsilon)^{1/2}}$$

$$= 2\pi\left(\frac{1}{\pi kT}\right)^{3/2}\varepsilon^{1/2}\mathrm{e}^{-\varepsilon/kT}\mathrm{d}\varepsilon = f(\varepsilon)\mathrm{d}\varepsilon \qquad (24.18)$$

The integral we need to evaluate is therefore

$$\int_0^\infty \sigma(\varepsilon)v_{\mathrm{rel}}f(\varepsilon)\mathrm{d}\varepsilon = 2\pi\left(\frac{1}{\pi kT}\right)^{3/2}\int_0^\infty \sigma(\varepsilon)\left(\frac{2\varepsilon}{\mu}\right)^{1/2}\varepsilon^{1/2}\mathrm{e}^{-\varepsilon/kT}\mathrm{d}\varepsilon$$

$$= \left(\frac{8}{\pi\mu kT}\right)^{1/2}\left(\frac{1}{kT}\right)\int_0^\infty \varepsilon\sigma(\varepsilon)\mathrm{e}^{-\varepsilon/kT}\mathrm{d}\varepsilon$$

To proceed, we introduce the approximation for $\sigma(\varepsilon)$ in eqn 24.13, and evaluate

$$\int_0^\infty \varepsilon\sigma(\varepsilon)\mathrm{e}^{-\varepsilon/kT}\mathrm{d}\varepsilon = \sigma\int_{\varepsilon_a}^\infty \varepsilon\left(1-\frac{\varepsilon_a}{\varepsilon}\right)\mathrm{e}^{-\varepsilon/kT}\mathrm{d}\varepsilon = (kT)^2\sigma\mathrm{e}^{-\varepsilon_a/kT}$$

We have made use of the fact that $\sigma = 0$ for $\varepsilon < \varepsilon_a$. It follows that

$$\int_0^\infty \sigma(\varepsilon)v_{\mathrm{rel}}f(\varepsilon)\mathrm{d}\varepsilon = \sigma\left(\frac{8kT}{\pi\mu}\right)^{1/2}\mathrm{e}^{-\varepsilon_a/kT}$$

as in eqn 24.14 (with $\varepsilon_a/kT = E_a/RT$).

Equation 24.14 has the Arrhenius form $k_2 = A\mathrm{e}^{-E_a/RT}$ provided the exponential temperature dependence dominates the weak square-root temperature dependence of the pre-exponential factor. It follows that we can identify the activation energy, E_a, with the minimum kinetic energy along the line of approach that is needed for reaction, and that the pre-exponential factor is a measure of the rate at which collisions occur in the gas.

(c) The steric requirement

The simplest procedure for calculating k_2 is to use for σ the values obtained for non-reactive collisions (for example, typically those obtained from viscosity measurements) or from tables of molecular radii. Table 24.1 compares some values of the pre-exponential factor calculated in this way with values obtained from Arrhenius plots (Section 22.5a). One of the reactions shows fair agreement between theory and

Synoptic table 24.1* Arrhenius parameters for gas-phase reactions

	$A/(\mathrm{dm^3\ mol^{-1}\ s^{-1}})$			
	Experiment	Theory	$E_a/(\mathrm{kJ\ mol^{-1}})$	P
$2\ \mathrm{NOCl} \rightarrow 2\ \mathrm{NO} + 2\ \mathrm{Cl}$	9.4×10^{9}	5.9×10^{10}	102	0.16
$2\ \mathrm{ClO} \rightarrow \mathrm{Cl_2} + \mathrm{O_2}$	6.3×10^{7}	2.5×10^{10}	0	2.5×10^{-3}
$\mathrm{H_2} + \mathrm{C_2H_4} \rightarrow \mathrm{C_2H_6}$	1.24×10^{6}	7.4×10^{11}	180	1.7×10^{-6}
$\mathrm{K} + \mathrm{Br_2} \rightarrow \mathrm{KBr} + \mathrm{Br}$	1.0×10^{12}	2.1×10^{11}	0	4.8

* More values are given in the *Data section*.

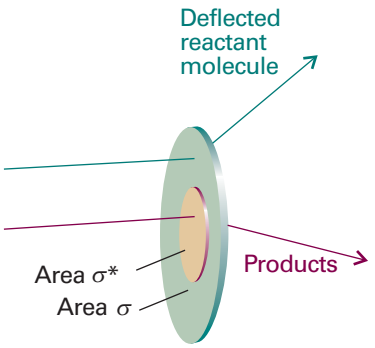

Fig. 24.4 The collision cross-section is the target area that results in simple deflection of the projectile molecule; the reaction cross-section is the corresponding area for chemical change to occur on collision.

experiment, but for others there are major discrepancies. In some cases the experimental values are orders of magnitude smaller than those calculated, which suggests that the collision energy is not the only criterion for reaction and that some other feature, such as the relative orientation of the colliding species, is important. Moreover, one reaction in the table has a pre-exponential factor larger than theory, which seems to indicate that the reaction occurs more quickly than the particles collide!

We can accommodate the disagreement between experiment and theory by introducing a **steric factor**, P, and expressing the **reactive cross-section**, σ^*, as a multiple of the collision cross-section, $\sigma^* = P\sigma$ (Fig. 24.4). Then the rate constant becomes

$$k_2 = P\sigma\left(\frac{8kT}{\pi\mu}\right)^{1/2} N_A e^{-E_a/RT} \qquad (24.19)$$

This expression has the form we anticipated in eqn 24.2. The steric factor is normally found to be several orders of magnitude smaller than 1.

Example 24.1 *Estimating a steric factor (1)*

Estimate the steric factor for the reaction $H_2 + C_2H_4 \rightarrow C_2H_6$ at 628 K given that the pre-exponential factor is 1.24×10^6 dm^3 mol^{-1} s^{-1}.

Method To calculate P, we need to calculate the pre-exponential factor, A, by using eqn 24.19 and then compare the answer with experiment: the ratio is P. Table 21.1 lists collision cross-sections for non-reactive encounters. The best way to estimate the collision cross-section for dissimilar spherical species is to calculate the collision diameter for each one (from $\sigma = \pi d^2$), to calculate the mean of the two diameters, and then to calculate the cross-section for that mean diameter. However, as neither species is spherical, a simpler but more approximate procedure is just to take the average of the two collision cross-sections.

Answer The reduced mass of the colliding pair is

$$\mu = \frac{m_1 m_2}{m_1 + m_2} = 3.12 \times 10^{-27} \text{ kg}$$

because $m_1 = 2.016$ u for H_2 and $m_2 = 28.05$ u for C_2H_4 (the atomic mass unit, 1 u, is defined inside the front cover). Hence

$$\left(\frac{8kT}{\pi\mu}\right)^{1/2} = 2.66 \times 10^3 \text{ m s}^{-1}$$

From Table 21.1, $\sigma(H_2) = 0.27$ nm^2 and $\sigma(C_2H_4) = 0.64$ nm^2, giving a mean collision cross-section of $\sigma = 0.46$ nm^2. Therefore,

$$A = \sigma\left(\frac{8kT}{\pi\mu}\right)^{1/2} N_A = 7.37 \times 10^{11} \text{ dm}^3 \text{ mol}^{-1} \text{ s}^{-1}$$

Experimentally $A = 1.24 \times 10^6$ dm^3 mol^{-1} s^{-1}, so it follows that $P = 1.7 \times 10^{-6}$. The very small value of P is one reason why catalysts are needed to bring this reaction about at a reasonable rate. As a general guide, the more complex the molecules, the smaller the value of P.

Self-test 24.1 It is found for the reaction $NO + Cl_2 \rightarrow NOCl + Cl$ that $A = 4.0 \times 10^9$ dm^3 mol^{-1} s^{-1} at 298 K. Use $\sigma(NO) = 0.42$ nm^2 and $\sigma(Cl_2) = 0.93$ nm^2 to estimate the P factor for the reaction. [0.018]

An example of a reaction for which it is possible to estimate the steric factor is $K + Br_2 \rightarrow KBr + Br$, with the experimental value $P = 4.8$. In this reaction, the distance of approach at which reaction occurs appears to be considerably larger than the distance needed for deflection of the path of the approaching molecules in a non-reactive collision. It has been proposed that the reaction proceeds by a **harpoon mechanism**. This brilliant name is based on a model of the reaction that pictures the K atom as approaching a Br_2 molecule, and when the two are close enough an electron (the harpoon) flips across from K to Br_2. In place of two neutral particles there are now two ions, so there is a Coulombic attraction between them: this attraction is the line on the harpoon. Under its influence the ions move together (the line is wound in), the reaction takes place, and KBr + Br emerge. The harpoon extends the cross-section for the reactive encounter, and the reaction rate is greatly underestimated by taking for the collision cross-section the value for simple mechanical contact between $K + Br_2$.

Example 24.2 *Estimating a steric factor (2)*

Estimate the value of P for the harpoon mechanism by calculating the distance at which it becomes energetically favourable for the electron to leap from K to Br_2.

Method We should begin by identifying all the contributions to the energy of interaction between the colliding species. There are three contributions to the energy of the process $K + Br_2 \rightarrow K^+ + Br_2^-$. The first is the ionization energy, I, of K. The second is the electron affinity, E_{ea}, of Br_2. The third is the Coulombic interaction energy between the ions when they have been formed: when their separation is R, this energy is $-e^2/4\pi\varepsilon_0 R$. The electron flips across when the sum of these three contributions changes from positive to negative (that is, when the sum is zero).

Answer The net change in energy when the transfer occurs at a separation R is

$$E = I - E_{ea} - \frac{e^2}{4\pi\varepsilon_0 R}$$

The ionization energy I is larger than E_{ea}, so E becomes negative only when R has decreased to less than some critical value R^* given by

$$\frac{e^2}{4\pi\varepsilon_0 R^*} = I - E_{ea}$$

When the particles are at this separation, the harpoon shoots across from K to Br_2, so we can identify the reactive cross-section as $\sigma^* = \pi R^{*2}$. This value of σ^* implies that the steric factor is

$$P = \frac{\sigma^*}{\sigma} = \frac{R^{*2}}{d^2} = \left\{ \frac{e^2}{4\pi\varepsilon_0 d(I - E_{ea})} \right\}^2$$

where $d = R(K) + R(Br_2)$. With $I = 420$ kJ mol^{-1} (corresponding to 7.0×10^{-19} J), $E_{ea} \approx 250$ kJ mol^{-1} (corresponding to 4.2×10^{-19} J), and $d = 400$ pm, we find $P = 4.2$, in good agreement with the experimental value (4.8).

Self-test 24.2 Estimate the value of P for the harpoon reaction between Na and Cl_2 for which $d \approx 350$ pm; take $E_{ea} \approx 230$ kJ mol^{-1}. [2.2]

Example 24.2 illustrates two points about steric factors. First, the concept of a steric factor is not wholly useless because in some cases its numerical value can be estimated.

Second (and more pessimistically) most reactions are much more complex than K + Br_2, and we cannot expect to obtain P so easily. What we need is a more powerful theory that lets us calculate, and not merely guess, its value. We go some way to setting up that theory in Section 24.4.

24.2 Diffusion-controlled reactions

Encounters between reactants in solution occur in a very different manner from encounters in gases. Reactant molecules have to jostle their way through the solvent, so their encounter frequency is considerably less than in a gas. However, because a molecule also migrates only slowly away from a location, two reactant molecules that encounter each other stay near each other for much longer than in a gas. This lingering of one molecule near another on account of the hindering presence of solvent molecules is called the **cage effect**. Such an encounter pair may accumulate enough energy to react even though it does not have enough energy to do so when it first forms. The activation energy of a reaction is a much more complicated quantity in solution than in a gas because the encounter pair is surrounded by solvent and we need to consider the energy of the entire local assembly of reactant and solvent molecules.

(a) Classes of reaction

The complicated overall process can be divided into simpler parts by setting up a simple kinetic scheme. We suppose that the rate of formation of an encounter pair AB is first-order in each of the reactants A and B:

$$\mathrm{A} + \mathrm{B} \rightarrow \mathrm{AB} \qquad v = k_\mathrm{d}[\mathrm{A}][\mathrm{B}] \tag{24.20a}$$

As we shall see, k_d (where the d signifies diffusion) is determined by the diffusional characteristics of A and B. The encounter pair can break up without reaction or it can go on to form products P. If we suppose that both processes are pseudofirst-order reactions (with the solvent perhaps playing a role), then we can write

$$\mathrm{AB} \rightarrow \mathrm{A} + \mathrm{B} \qquad v = k'_\mathrm{d}[\mathrm{AB}] \tag{24.20b}$$

and

$$\mathrm{AB} \rightarrow \mathrm{P} \qquad v = k_\mathrm{a}[\mathrm{AB}] \tag{24.20c}$$

The concentration of AB can now be found from the equation for the net rate of change of concentration of AB:

$$\frac{\mathrm{d}[\mathrm{AB}]}{\mathrm{d}t} = k_\mathrm{d}[\mathrm{A}][\mathrm{B}] - k'_\mathrm{d}[\mathrm{AB}] - k_\mathrm{a}[\mathrm{AB}] \approx 0 \tag{24.21}$$

where we have applied the steady-state approximation. This expression solves to

$$[\mathrm{AB}] = \frac{k_\mathrm{d}[\mathrm{A}][\mathrm{B}]}{k_\mathrm{a} + k'_\mathrm{d}} \tag{24.22}$$

The rate of formation of products is therefore

$$\frac{\mathrm{d}[\mathrm{P}]}{\mathrm{d}t} \approx k_\mathrm{a}[\mathrm{AB}] = k_2[\mathrm{A}][\mathrm{B}] \qquad k_2 = \frac{k_\mathrm{a}k_\mathrm{d}}{k_\mathrm{a} + k'_\mathrm{d}} \tag{24.23}$$

Two limits can now be distinguished. If the rate of separation of the unreacted encounter pair is much slower than the rate at which it forms products, then $k'_\mathrm{d} \ll k_\mathrm{a}$ and the effective rate constant is

Synoptic table 24.2* Arrhenius parameters for reactions in solution

	Solvent	$A/(\text{dm}^3\ \text{mol}^{-1}\ \text{s}^{-1})$	$E_a/(\text{kJ mol}^{-1})$
$(CH_3)_3CCl$ solvolysis	Water	7.1×10^{16}	100
	Ethanol	3.0×10^{13}	112
	Chloroform	1.4×10^{4}	45
CH_3CH_2Br	Ethanol	4.3×10^{11}	90

* More values are given in the *Data section*.

$$k_2 \approx \frac{k_a k_d}{k_a} = k_d \tag{24.24}$$

In this **diffusion-controlled limit**, the rate of reaction is governed by the rate at which the reactant molecules diffuse through the solvent. An indication that a reaction is diffusion-controlled is that its rate constant is of the order of 10^9 $\text{dm}^3\ \text{mol}^{-1}\ \text{s}^{-1}$ or greater. Because the combination of radicals involves very little activation energy, radical and atom recombination reactions are often diffusion-controlled.

An **activation-controlled reaction** arises when a substantial activation energy is involved in the reaction AB → P. Then $k_a \ll k'_d$ and

$$k_2 \approx \frac{k_a k_d}{k'_d} = k_a K \tag{24.25}$$

where K is the equilibrium constant for A + B ⇌ AB. In this limit, the reaction proceeds at the rate at which energy accumulates in the encounter pair from the surrounding solvent. Some experimental data are given in Table 24.2.

(b) Diffusion and reaction

The rate of a diffusion-controlled reaction is calculated by considering the rate at which the reactants diffuse together. As shown in the *Justification* below, the rate constant for a reaction in which the two reactant molecules react if they come within a distance R^* of one another is

$$k_d = 4\pi R^* D N_A \tag{24.26}$$

where D is the sum of the diffusion coefficients the two reactant species in the solution.

Justification 24.3 *Solution of the radial diffusion equation*

From the form of the diffusion equation (Section 21.10) corresponding to motion in three dimensions, $D_B \nabla^2[B] = \partial[B]/\partial t$, the concentration of B when the system has reached a steady state ($\partial[B]/\partial t = 0$) satisfies $\nabla^2[B]_r = 0$, where the subscript r signifies a quantity that varies with the distance r. For a spherically symmetrical system, ∇^2 can be replaced by radial derivatives alone (see Table 8.1), so the equation satisfied by $[B]_r$ is

$$\frac{d^2[B]_r}{dr^2} + \frac{2}{r}\frac{d[B]_r}{dr} = 0 \tag{24.27}$$

The general solution of this equation is

$$[B]_r = a + \frac{b}{r} \tag{24.28}$$

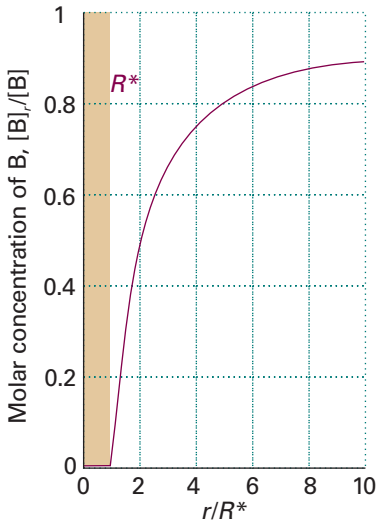

Fig. 24.5 The concentration profile for reaction in solution when a molecule B diffuses towards another reactant molecule and reacts if it reaches R^*.

as may be verified by substitution. We need two boundary conditions to pin down the values of the two constants. One condition is that $[B]_r$ has its bulk value [B] as $r \to \infty$. The second condition is that the concentration of B is zero at $r = R^*$, the distance at which reaction occurs. It follows that $a = [B]$ and $b = -R^*[B]$, and hence that (for $r \geq R^*$)

$$[B]_r = \left(1 + \frac{R^*}{r}\right)[B] \tag{24.29}$$

Figure 24.5 illustrates the variation of concentration expressed by this equation.

The rate of reaction is the (molar) flux, J, of the reactant B towards A multiplied by the area of the spherical surface of radius R^*:

$$\text{Rate of reaction} = 4\pi R^{*2} J \tag{24.30}$$

From Fick's first law (eqn 21.17), the flux towards A is proportional to the concentration gradient, so at a radius R^*:

$$J = D_B \left(\frac{d[B]_r}{dr}\right)_{r=R^*} = \frac{D_B[B]}{R^*} \tag{24.31}$$

(A sign change has been introduced because we are interested in the flux towards decreasing values of r.) When this condition is substituted into the previous equation we obtain

$$\text{Rate of reaction} = 4\pi R^* D_B[B] \tag{24.32}$$

The rate of the diffusion-controlled reaction is equal to the average flow of B molecules to all the A molecules in the sample. If the bulk concentration of A is [A], the number of A molecules in the sample of volume V is $N_A[A]V$; the global flow of all B to all A is therefore $4\pi R^* D_B N_A[A][B]V$. Because it is unrealistic to suppose that all A are stationary; we replace D_B by the sum of the diffusion coefficients of the two species and write $D = D_A + D_B$. Then the rate of change of concentration of AB is

$$\frac{d[AB]}{dt} = 4\pi R^* D N_A[A][B] \tag{24.33}$$

Hence, the diffusion-controlled rate constant is as given in eqn 24.26.

We can take eqn 24.26 further by incorporating the Stokes–Einstein equation (eqn 21.66) relating the diffusion constant and the hydrodynamic radius R_A and R_B of each molecule in a medium of viscosity η:

$$D_A = \frac{kT}{6\pi\eta R_A} \qquad D_B = \frac{kT}{6\pi\eta R_B} \tag{24.34}$$

As these relations are approximate, little extra error is introduced if we write $R_A = R_B = \frac{1}{2}R^*$, which leads to

$$k_d = \frac{8RT}{3\eta} \tag{24.35}$$

(The R in this equation is the gas constant.) The radii have cancelled because, although the diffusion constants are smaller when the radii are large, the reactive collision radius is larger and the particles need travel a shorter distance to meet. In this approximation, the rate constant is independent of the identities of the reactants, and depends only on the temperature and the viscosity of the solvent.

Illustration 24.1 *Estimating a diffusional rate constant*

The rate constant for the recombination of I atoms in hexane at 298 K, when the viscosity of the solvent is 0.326 cP (with $1\ \mathrm{P} = 10^{-1}\ \mathrm{kg\ m^{-1}\ s^{-1}}$) is

$$k_{\mathrm{d}} = \frac{8 \times (8.3145\ \mathrm{J\ K^{-1}\ mol^{-1}}) \times (298\ \mathrm{K})}{3 \times (3.26 \times 10^{-4}\ \mathrm{kg\ m^{-1}\ s^{-1}})} = 2.0 \times 10^{7}\ \mathrm{m^3\ mol^{-1}\ s^{-1}}$$

where we have used $1\ \mathrm{J} = 1\ \mathrm{kg\ m^2\ s^{-2}}$. Because $1\ \mathrm{m^3} = 10^3\ \mathrm{dm^3}$, this result corresponds to $2.0 \times 10^{10}\ \mathrm{dm^3\ mol^{-1}\ s^{-1}}$. The experimental value is $1.3 \times 10^{10}\ \mathrm{dm^3\ mol^{-1}\ s^{-1}}$, so the agreement is very good considering the approximations involved.

24.3 The material balance equation

The diffusion of reactants plays an important role in many chemical processes, such as the diffusion of O_2 molecules into red blood corpuscles and the diffusion of a gas towards a catalyst. We can have a glimpse of the kinds of calculations involved by considering the diffusion equation (Section 21.10) generalized to take into account the possibility that the diffusing, convecting molecules are also reacting.

(a) The formulation of the equation

Consider a small volume element in a chemical reactor (or a biological cell). The net rate at which J molecules enter the region by diffusion and convection is given by eqn 21.71:

$$\frac{\partial[\mathrm{J}]}{\partial t} = D\frac{\partial^2[\mathrm{J}]}{\partial x^2} - v\frac{\partial[\mathrm{J}]}{\partial x} \tag{24.36}$$

The net rate of change of molar concentration due to chemical reaction is

$$\frac{\partial[\mathrm{J}]}{\partial t} = -k[\mathrm{J}] \tag{24.37}$$

if we suppose that J disappears by a pseudofirst-order reaction. Therefore, the overall rate of change of the concentration of J is

$$\frac{\partial[\mathrm{J}]}{\partial t} = \underbrace{D\frac{\partial^2[\mathrm{J}]}{\partial x^2}}_{\substack{\text{Spread due to}\\ \text{non-uniform}\\ \text{concentration}}} - \underbrace{v\frac{\partial[\mathrm{J}]}{\partial x}}_{\substack{\text{Change}\\ \text{due to}\\ \text{convection}}} - \underbrace{k[\mathrm{J}]}_{\substack{\text{Loss}\\ \text{due to}\\ \text{reaction}}} \tag{24.38}$$

Equation 24.38 is called the **material balance equation**. If the rate constant is large, then [J] will decline rapidly. However, if the diffusion constant is large, then the decline can be replenished as J diffuses rapidly into the region. The convection term, which may represent the effects of stirring, can sweep material either into or out of the region according to the signs of v and the concentration gradient $\partial[\mathrm{J}]/\partial x$.

(b) Solutions of the equation

The material balance equation is a second-order partial differential equation and is far from easy to solve in general. Some idea of how it is solved can be obtained by considering the special case in which there is no convective motion (as in an unstirred reaction vessel):

$$\frac{\partial[\mathrm{J}]}{\partial t} = D\frac{\partial^2[\mathrm{J}]}{\partial x^2} - k[\mathrm{J}] \tag{24.39}$$

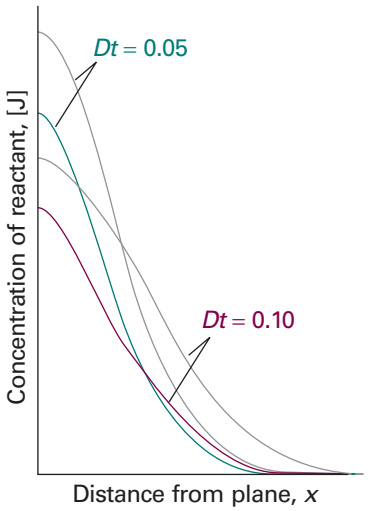

Fig. 24.6 The concentration profiles for a diffusing, reacting system (for example, a column of solution) in which one reactant is initially in a layer at $x = 0$. In the absence of reaction (grey lines) the concentration profiles are the same as in Fig. 21.26.

Exploration Use the interactive applet found in the *Living graphs* section of the text's web site to explore the effect of varying the value of the rate constant k on the spatial variation of [J] for a constant value of the diffusion constant D.

As may be verified by susbtitution, if the solution of this equation in the absence of reaction (that is, for $k = 0$) is [J], then the solution in the presence of reaction ($k > 0$) is

$$[\mathrm{J}]^\star = k\int_0^t [\mathrm{J}]\mathrm{e}^{-kt}\,\mathrm{d}t + [\mathrm{J}]\mathrm{e}^{-kt} \tag{24.40}$$

We have already met one solution of the diffusion equation in the absence of reaction: eqn 21.71 is the solution for a system in which initially a layer of $n_0 N_\mathrm{A}$ molecules is spread over a plane of area A:

$$[\mathrm{J}] = \frac{n_0 \mathrm{e}^{-x^2/4Dt}}{A(\pi Dt)^{1/2}} \tag{24.41}$$

When this expression is substituted into eqn 24.40 and the integral is evaluated numerically, we obtain the concentration of J as it diffuses away from its initial surface layer and undergoes reaction in the solution above (Fig. 24.6).

Even this relatively simple example has led to an equation that is difficult to solve, and only in some special cases can the full material balance equation be solved analytically. Most modern work on reactor design and cell kinetics uses numerical methods to solve the equation, and detailed solutions for realistic environments, such as vessels of different shapes (which influence the boundary conditions on the solutions) and with a variety of inhomogeneously distributed reactants can be obtained reasonably easily.

Transition state theory

We saw in Section 22.5b that an activated complex forms between reactants as they collide and begin to assume the nuclear and electronic configurations characteristic of products. We also saw that the change in potential energy associated with formation of the activated complex accounts for the activation energy of the reaction. We now consider a more detailed calculation of rate constants which uses the concepts of statistical thermodynamics developed in Chapter 17. The approach we describe, which is called **transition state theory** (also widely referred to as *activated complex theory*), has the advantage that a quantity corresponding to the steric factor appears automatically, and P does not need to be grafted on to an equation as an afterthought. Transition state theory is an attempt to identify the principal features governing the size of a rate constant in terms of a model of the events that take place during the reaction. There are several approaches to the calculation, all of which lead to the same final expression (see *Further reading*); here we present the simplest approach.

Comment 24.3
This chapter inevitably puts heavy demands on the letter K; the various meanings are summarized in Table 24.3 at the end of the chapter.

24.4 The Eyring equation

Transition state theory pictures a reaction between A and B as proceeding through the formation of an activated complex, $\mathrm{C}^\ddagger$, in a rapid pre-equilibrium (Fig. 24.7):

$$\mathrm{A} + \mathrm{B} \rightleftharpoons \mathrm{C}^\ddagger \qquad K^\ddagger = \frac{p_{\mathrm{C}^\ddagger} p^\ominus}{p_\mathrm{A} p_\mathrm{B}} \tag{24.42}$$

When we express the partial pressures, p_J, in terms of the molar concentrations, [J], by using $p_\mathrm{J} = RT[\mathrm{J}]$, the concentration of activated complex is related to the (dimensionless) equilibrium constant by

$$[\mathrm{C}^\ddagger] = \frac{RT}{p^\ominus} K^\ddagger [\mathrm{A}][\mathrm{B}] \tag{24.43}$$

The activated complex falls apart by unimolecular decay into products, P, with a rate constant $k^{\ddagger}$:

$$C^{\ddagger} \rightarrow P \qquad v = k^{\ddagger}[C^{\ddagger}] \tag{24.44}$$

It follows that

$$v = k_2[A][B] \qquad k_2 = \frac{RT}{p^{\ominus}} k^{\ddagger} K^{\ddagger} \tag{24.45}$$

Our task is to calculate the unimolecular rate constant $k^{\ddagger}$ and the equilibrium constant $K^{\ddagger}$.

(a) The rate of decay of the activated complex

An activated complex can form products if it passes through the **transition state**, the arrangement the atoms must achieve in order to convert to products (Section 22.5b). If its vibration-like motion along the reaction coordinate occurs with a frequency ν, then the frequency with which the cluster of atoms forming the complex approaches the transition state is also ν. However, it is possible that not every oscillation along the reaction coordinate takes the complex through the transition state. For instance, the centrifugal effect of rotations might also be an important contribution to the break-up of the complex, and in some cases the complex might be rotating too slowly, or rotating rapidly but about the wrong axis. Therefore, we suppose that the rate of passage of the complex through the transition state is proportional to the vibrational frequency along the reaction coordinate, and write

$$k^{\ddagger} = \kappa\nu \tag{24.46}$$

where κ is the **transmission coefficient**. In the absence of information to the contrary, κ is assumed to be about 1.

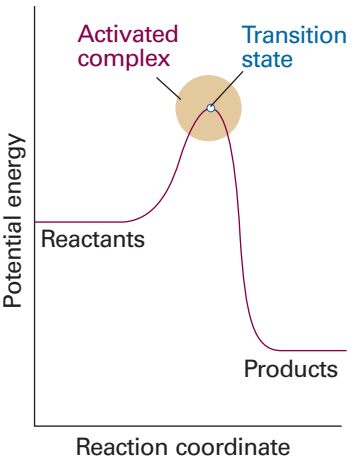

Fig. 24.7 A reaction profile. The horizontal axis is the reaction coordinate, and the vertical axis is potential energy. The activated complex is the region near the potential maximum, and the transition state corresponds to the maximum itself.

(b) The concentration of the activated complex

We saw in Section 17.8 how to calculate equilibrium constants from structural data. Equation 17.54 of that section can be used directly, which in this case gives

$$K^{\ddagger} = \frac{N_A q^{\ominus}_{C^{\ddagger}}}{q^{\ominus}_A q^{\ominus}_B} e^{-\Delta E_0/RT} \tag{24.47}$$

where $p^{\ominus} = 1$ bar and

$$\Delta E_0 = E_0(C^{\ddagger}) - E_0(A) - E_0(B) \tag{24.48}$$

The $q^{\ominus}_J$ are the standard molar partition functions, as defined in Section 17.1. Note that the units of N_A and the q_J are mol^{-1}, so $K^{\ddagger}$ is dimensionless (as is appropriate for an equilibrium constant).

In the final step of this part of the calculation, we focus attention on the partition function of the activated complex. We have already assumed that a vibration of the activated complex $C^{\ddagger}$ tips it through the transition state. The partition function for this vibration is

$$q = \frac{1}{1 - e^{-h\nu/kT}} \tag{24.49a}$$

where ν is its frequency (the same frequency that determines $k^{\ddagger}$). This frequency is much lower than for an ordinary molecular vibration because the oscillation corresponds to the complex falling apart (Fig. 24.8), so the force constant is very low.

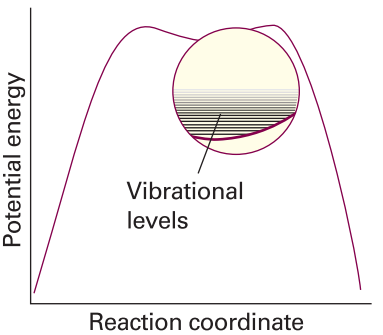

Fig. 24.8 In an elementary depiction of the activated complex close to the transition state, there is a broad, shallow dip in the potential energy surface along the reaction coordinate. The complex vibrates harmonically and almost classically in this well. However, this depiction is an oversimplification, for in many cases there is no dip at the top of the barrier, and the curvature of the potential energy, and therefore the force constant, is negative. Formally, the vibrational frequency is then imaginary. We ignore this problem here, but see *Further reading*.

Therefore, provided that $h\nu/kT \ll 1$, the exponential may be expanded and the partition function reduces to

$$q = \frac{1}{1 - \left(1 - \dfrac{h\nu}{kT} + \cdots\right)} \approx \frac{kT}{h\nu} \tag{24.49b}$$

We can therefore write

$$q_{C^\ddagger} \approx \frac{kT}{h\nu}\bar{q}_{C^\ddagger} \tag{24.50}$$

where $\bar{q}$ denotes the partition function for all the other modes of the complex. The constant $K^\ddagger$ is therefore

$$K^\ddagger = \frac{kT}{h\nu}\bar{K}^\ddagger \qquad \bar{K}^\ddagger = \frac{N_A\bar{q}^\ominus_{C^\ddagger}}{q^\ominus_A q^\ominus_B}e^{-\Delta E_0/RT} \tag{24.51}$$

with $\bar{K}^\ddagger$ a kind of equilibrium constant, but with one vibrational mode of $C^\ddagger$ discarded.

(c) The rate constant

We can now combine all the parts of the calculation into

$$k_2 = k^\ddagger\frac{RT}{p^\ominus}K^\ddagger = \kappa\nu\frac{kT}{h\nu}\frac{RT}{p^\ominus}\bar{K}^\ddagger \tag{24.52}$$

At this stage the unknown frequencies ν cancel and, after writing $\bar{K}^\ddagger_c = (RT/p^\ominus)\bar{K}^\ddagger$, we obtain the **Eyring equation**:

$$k_2 = \kappa\frac{kT}{h}\bar{K}^\ddagger_c \tag{24.53}$$

The factor $\bar{K}^\ddagger_c$ is given by eqn 24.51 and the definition $\bar{K}^\ddagger_c = (RT/p^\ominus)\bar{K}^\ddagger$ in terms of the partition functions of A, B, and $C^\ddagger$, so in principle we now have an explicit expression for calculating the second-order rate constant for a bimolecular reaction in terms of the molecular parameters for the reactants and the activated complex and the quantity κ.

The partition functions for the reactants can normally be calculated quite readily, using either spectroscopic information about their energy levels or the approximate expressions set out in Table 17.3. The difficulty with the Eyring equation, however, lies in the calculation of the partition function of the activated complex: $C^\ddagger$ is difficult to investigate spectroscopically (but see Section 24.9), and in general we need to make assumptions about its size, shape, and structure. We shall illustrate what is involved in one simple but significant case.

(d) The collision of structureless particles

Consider the case of two structureless particles A and B colliding to give an activated complex that resembles a diatomic molecule. Because the reactants J = A, B are structureless 'atoms', the only contributions to their partition functions are the translational terms:

$$q^\ominus_J = \frac{V^\ominus_m}{\Lambda_J^3} \qquad \Lambda_J = \frac{h}{(2\pi m_J kT)^{1/2}} \qquad V^\ominus_m = \frac{RT}{p^\ominus} \tag{24.54}$$

The activated complex is a diatomic cluster of mass $m_C = m_A + m_B$ and moment of inertia I. It has one vibrational mode, but that mode corresponds to motion along the

reaction coordinate and therefore does not appear in $\bar{q}_{C^\ddagger}$. It follows that the standard molar partition function of the activated complex is

$$q^{\ominus}_{C^\ddagger} = \left(\frac{2IkT}{\hbar^2}\right)\frac{V^{\ominus}_m}{\Lambda^3_{C^\ddagger}} \tag{24.55}$$

The moment of inertia of a diatomic molecule of bond length r is μr^2, where $\mu = m_A m_B/(m_A + m_B)$ is the effective mass, so the expression for the rate constant is

$$\begin{aligned} k_2 &= \kappa\frac{kT}{h}\frac{RT}{p^{\ominus}}\left(\frac{N_A\Lambda^3_A\Lambda^3_B}{\Lambda^3_{C^\ddagger}V^{\ominus}_m}\right)\left(\frac{2IkT}{\hbar^2}\right)e^{-\Delta E_0/RT} \\ &= \kappa\frac{kT}{h}N_A\left(\frac{\Lambda_A\Lambda_B}{\Lambda_{C^\ddagger}}\right)\left(\frac{2IkT}{\hbar^2}\right)e^{-\Delta E_0/RT} \\ &= \kappa N_A\left(\frac{8kT}{\pi\mu}\right)^{1/2}\pi r^2 e^{-\Delta E_0/RT} \end{aligned} \tag{24.56}$$

Finally, by identifying $\kappa\pi r^2$ as the reactive cross-section $\sigma^\star$, we arrive at precisely the same expression as that obtained from simple collision theory (eqn 24.14).

24.5 Thermodynamic aspects

The statistical thermodynamic version of transition state theory rapidly runs into difficulties because only in some cases is anything known about the structure of the activated complex. However, the concepts that it introduces, principally that of an equilibrium between the reactants and the activated complex, have motivated a more general, empirical approach in which the activation process is expressed in terms of thermodynamic functions.

(a) Activation parameters

If we accept that $\bar{K}^\ddagger$ is an equilibrium constant (despite one mode of $C^\ddagger$ having been discarded), we can express it in terms of a **Gibbs energy of activation**, $\Delta^\ddagger G$, through the definition

$$\Delta^\ddagger G = -RT\ln\bar{K}^\ddagger \tag{24.57}$$

(All the $\Delta^\ddagger X$ in this section are *standard* thermodynamic quantities, $\Delta^\ddagger X^{\ominus}$, but we shall omit the standard state sign to avoid overburdening the notation). Then the rate constant becomes

$$k_2 = \kappa\frac{kT}{h}\frac{RT}{p^{\ominus}}e^{-\Delta^\ddagger G/RT} \tag{24.58}$$

Because $G = H - TS$, the Gibbs energy of activation can be divided into an **entropy of activation**, $\Delta^\ddagger S$, and an **enthalpy of activation**, $\Delta^\ddagger H$, by writing

$$\Delta^\ddagger G = \Delta^\ddagger H - T\Delta^\ddagger S \tag{24.59}$$

When eqn 24.59 is used in eqn 24.58 and κ is absorbed into the entropy term, we obtain

$$k_2 = Be^{\Delta^\ddagger S/R}e^{-\Delta^\ddagger H/RT} \qquad B = \frac{kT}{h}\frac{RT}{p^{\ominus}} \tag{24.60}$$

The formal definition of activation energy, $E_a = RT^2(\partial\ln k/\partial T)$, then gives $E_a = \Delta^\ddagger H + 2RT$, so

$$k_2 = e^2Be^{\Delta^\ddagger S/R}e^{-E_a/RT} \tag{24.61}$$

Comment 24.4

For reactions of the type A + B ⇌ P in the gas phase, $E_a = \Delta^\ddagger H + 2RT$. For these reactions in solution, $E_a = \Delta^\ddagger H + RT$.

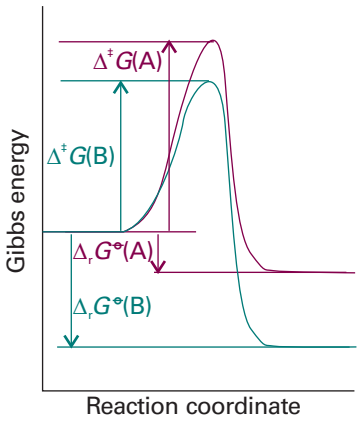

Fig. 24.9 For a related series of reactions, as the magnitude of the standard reaction Gibbs energy increases, so the activation barrier decreases. The approximate linear correlation between $\Delta^{\ddagger}G$ and $\Delta_r G^{\ominus}$ is the origin of linear free energy relations.

from which it follows that the Arrhenius factor A can be identified as

$$A = e^2 B e^{\Delta^{\ddagger}S/R} \tag{24.62}$$

The entropy of activation is negative because two reactant species come together to form one species. However, if there is a reduction in entropy below what would be expected for the simple encounter of A and B, then A will be smaller than that expected on the basis of simple collision theory. Indeed, we can identify that additional reduction in entropy, $\Delta^{\ddagger}S_{\text{steric}}$, as the origin of the steric factor of collision theory, and write

$$P = e^{\Delta^{\ddagger}S_{\text{steric}}/R} \tag{24.63}$$

Thus, the more complex the steric requirements of the encounter, the more negative the value of $\Delta^{\ddagger}S_{\text{steric}}$, and the smaller the value of P.

Gibbs energies, enthalpies, entropies, volumes, and heat capacities of activation are widely used to report experimental reaction rates, especially for organic reactions in solution. They are encountered when relationships between equilibrium constants and rates of reaction are explored using **correlation analysis**, in which ln K (which is equal to $-\Delta_r G^{\ominus}/RT$) is plotted against ln k (which is proportional to $-\Delta^{\ddagger}G/RT$). In many cases the correlation is linear, signifying that, as the reaction becomes thermodynamically more favourable, its rate constant increases (Fig. 24.9). This linear correlation is the origin of the alternative name **linear free energy relation** (LFER; see *Further reading*).

(b) Reactions between ions

The thermodynamic version of transition state theory simplifies the discussion of reactions in solution. The statistical thermodynamic theory is very complicated to apply because the solvent plays a role in the activated complex. In the thermodynamic approach we combine the rate law

$$\frac{d[P]}{dt} = k^{\ddagger}[C^{\ddagger}] \tag{24.64}$$

with the thermodynamic equilibrium constant

$$K = \frac{a_{C^{\ddagger}}}{a_A a_B} = K_{\gamma}\frac{[C^{\ddagger}]}{[A][B]} \qquad K_{\gamma} = \frac{\gamma_{C^{\ddagger}}}{\gamma_A \gamma_B} \tag{24.65}$$

Then

$$\frac{d[P]}{dt} = k_2[A][B] \qquad k_2 = \frac{k^{\ddagger}K}{K_{\gamma}} \tag{24.66}$$

If k_2° is the rate constant when the activity coefficients are 1 (that is, $k_2^{\circ} = k^{\ddagger}K$), we can write

$$k_2 = \frac{k_2^{\circ}}{K_{\gamma}} \tag{24.67}$$

At low concentrations the activity coefficients can be expressed in terms of the ionic strength, I, of the solution by using the Debye–Hückel limiting law (Section 5.9, particularly eqn 5.69) in the form

$$\log \gamma_J = -Az_J^2 I^{1/2} \tag{24.68}$$

with $A = 0.509$ in aqueous solution at 298 K. Then

$$\log k_2 = \log k_2^{\circ} - A\{z_A^2 + z_B^2 - (z_A + z_B)^2\}I^{1/2} = \log k_2^{\circ} + 2Az_A z_B I^{1/2} \tag{24.69}$$

The charge numbers of A and B are z_A and z_B, so the charge number of the activated complex is $z_A + z_B$; the z_J are positive for cations and negative for anions.

Equation 24.69 expresses the **kinetic salt effect**, the variation of the rate constant of a reaction between ions with the ionic strength of the solution (Fig. 24.10). If the reactant ions have the same sign (as in a reaction between cations or between anions), then increasing the ionic strength by the addition of inert ions increases the rate constant. The formation of a single, highly charged ionic complex from two less highly charged ions is favoured by a high ionic strength because the new ion has a denser ionic atmosphere and interacts with that atmosphere more strongly. Conversely, ions of opposite charge react more slowly in solutions of high ionic strength. Now the charges cancel and the complex has a less favourable interaction with its atmosphere than the separated ions.

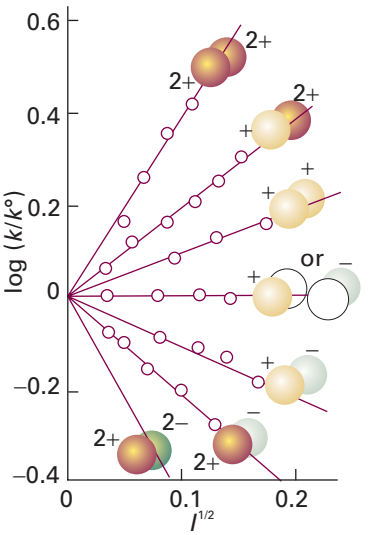

Fig. 24.10 Experimental tests of the kinetic salt effect for reactions in water at 298 K. The ion types are shown as spheres, and the slopes of the lines are those given by the Debye–Hückel limiting law and eqn 24.69.

Example 24.3 *Analysing the kinetic salt effect*

The rate constant for the base hydrolysis of $[CoBr(NH_3)_5]^{2+}$ varies with ionic strength as tabulated below. What can be deduced about the charge of the activated complex in the rate-determining stage?

I	0.0050	0.0100	0.0150	0.0200	0.0250	0.0300
$k/k°$	0.718	0.631	0.562	0.515	0.475	0.447

Method According to eqn 24.69, plot $\log(k/k°)$ against $I^{1/2}$, when the slope will give $1.02 z_A z_B$, from which we can infer the charges of the ions involved in the formation of the activated complex.

Answer Form the following table:

I	0.0050	0.0100	0.0150	0.0200	0.0250	0.0300
$I^{1/2}$	0.071	0.100	0.122	0.141	0.158	0.173
$\log(k/k°)$	−0.14	−0.20	−0.25	−0.29	−0.32	−0.35

These points are plotted in Fig. 24.11. The slope of the (least squares) straight line is −2.04, indicating that $z_A z_B = -2$. Because $z_A = -1$ for the OH^- ion, if that ion is involved in the formation of the activated complex, then the charge number of the second ion is +2. This analysis suggests that the pentaamminebromocobalt(III) cation participates in the formation of the activated complex. The rate constant is also influenced by the relative permittivity of the medium.

Self-test 24.3 An ion of charge number +1 is known to be involved in the activated complex of a reaction. Deduce the charge number of the other ion from the following data:

I	0.0050	0.010	0.015	0.020	0.025	0.030
$k/k°$	0.930	0.902	0.884	0.867	0.853	0.841

[−1]

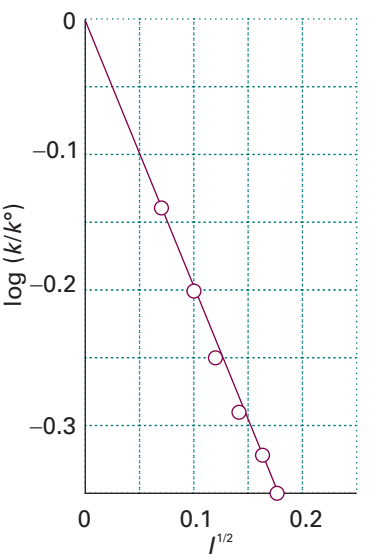

Fig. 24.11 The experimental ionic strength dependence of the rate constant of a hydrolysis reaction: the slope gives information about the charge types involved in the activated complex of the rate-determining step. See Example 24.3.

The dynamics of molecular collisions

We now come to the third and most detailed level of our examination of the factors that govern the rates of reactions.

24.6 Reactive collisions

Molecular beams allow us to study collisions between molecules in preselected energy states, and can be used to determine the states of the products of a reactive collision. Information of this kind is essential if a full picture of the reaction is to be built, because the rate constant is an average over events in which reactants in different initial states evolve into products in their final states.

(a) Experimental probes of reactive collisions

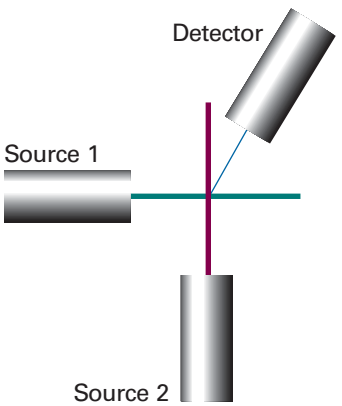

Fig. 24.12 In a crossed-beam experiment, state-selected molecules are generated in two separate sources, and are directed perpendicular to one another. The detector responds to molecules (which may be product molecules if chemical reaction occurs) scattered into a chosen direction.

Detailed experimental information about the intimate processes that occur during reactive encounters comes from molecular beams, especially crossed molecular beams (Fig. 24.12). The detector for the products of the collision of two beams can be moved to different angles, so the angular distribution of the products can be determined. Because the molecules in the incoming beams can be prepared with different energies (for example, with different translational energies by using rotating sectors and supersonic nozzles, with different vibrational energies by using selective excitation with lasers, as shown in Section 24.9b, and with different orientations (by using electric fields), it is possible to study the dependence of the success of collisions on these variables and to study how they affect the properties of the outcoming product molecules.

One method for examining the energy distribution in the products is **infrared chemiluminescence**, in which vibrationally excited molecules emit infrared radiation as they return to their ground states. By studying the intensities of the infrared emission spectrum, the populations of the vibrational states may be determined (Fig. 24.13). Another method makes use of **laser-induced fluorescence**. In this technique, a laser is used to excite a product molecule from a specific vibration-rotation level; the intensity of the fluorescence from the upper state is monitored and interpreted in terms of the population of the initial vibration-rotation state. When the molecules being studied do not fluoresce efficiently, coherent anti-Stokes Raman spectroscopy (CARS, Section 13.16) can be used to monitor the progress of reaction. **Multiphoton ionization** (MPI) techniques are also good alternatives for the study of weakly fluorescing molecules. In MPI, the absorption of several photons by a molecule results in ionization if the total photon energy is greater than the ionization energy of the molecule. One or more pulsed lasers are used to generate the molecular ions, which are commonly detected by time-of-flight mass spectrometry (TOF-MS, Section 19.2). The angular distribution of products can also be determined by **reaction product imaging**. In this technique, product ions are accelerated by an electric field towards a phosphorescent screen and the light emitted from specific spots where the ions struck the screen is imaged by a charge-coupled device (CCD, *Further information* 13.1). An important variant of MPI is **resonant multiphoton ionization** (REMPI), in which one or more photons promote a molecule to an electronically excited state and then additional photons are used to generate ions from the excited state. The power of REMPI lies in the fact that the experimenter can choose which reactant or product to study by tuning the laser frequency to the electronic absorption band of a specific molecule.

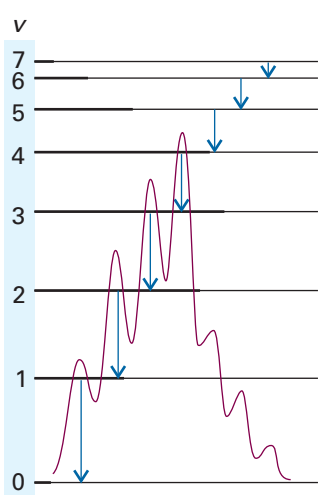

Fig. 24.13 Infrared chemiluminescence from CO produced in the reaction O + CS → CO + S arises from the non-equilibrium populations of the vibrational states of CO and the radiative relaxation to equilibrium.

(b) State-to-state dynamics

The concept of collision cross-section was introduced in connection with collision theory in Section 24.1, where we saw that the second-order rate constant, k_2, can be expressed as a Boltzmann-weighted average of the reactive collision cross-section and the relative speed of approach. We shall write eqn 24.12 as

$$k_2 = \langle \sigma v_{\text{rel}} \rangle N_{\text{A}} \tag{24.70}$$

where the angle brackets denote a Boltzmann average. Molecular beam studies provide a more sophisticated version of this quantity, for they provide the **state-to-state cross-section**, $\sigma_{nn'}$, and hence the **state-to-state rate constant**, $k_{nn'}$:

$$k_{nn'} = \langle \sigma_{nn'} v_{\text{rel}} \rangle N_{\text{A}} \tag{24.71}$$

The rate constant k_2 is the sum of the state-to-state rate constant over all final states (because a reaction is successful whatever the final state of the products) and over a Boltzmann-weighted sum of initial states (because the reactants are initially present with a characteristic distribution of populations at a temperature T):

$$k_2 = \sum_{n,n'} k_{nn'}(T) f_n(T) \tag{24.72}$$

where $f_n(T)$ is the Boltzmann factor at a temperature T. It follows that, if we can determine or calculate the state-to-state cross-sections for a wide range of approach speeds and initial and final states, then we have a route to the calculation of the rate constant for the reaction.

24.7 Potential energy surfaces

One of the most important concepts for discussing beam results and calculating the state-to-state collision cross-section is the **potential energy surface** of a reaction, the potential energy as a function of the relative positions of all the atoms taking part in the reaction. Potential energy surfaces may be constructed from experimental data, with the techniques described in Section 24.6, and from results of quantum chemical calculations (Section 11.7). The theoretical method requires the systematic calculation of the energies of the system in a large number of geometrical arrangements. Special computational techniques are used to take into account electron correlation, which arises from instantaneous interactions between electrons as they move closer to and farther from each other in molecule or molecular cluster. Techniques that incorporate electron correlation are very time-consuming and, consequently, only reactions between relatively small particles, such as the reactions $H + H_2 \rightarrow H_2 + H$ and $H + H_2O \rightarrow OH + H_2$, are amenable to this type of theoretical treatment. An alternative is to use semi-empirical methods, in which results of calculations and experimental parameters are used to construct the potential energy surface.

To illustrate the features of a potential energy surface we consider the collision between an H atom and an H_2 molecule. Detailed calculations show that the approach of an atom along the H—H axis requires less energy for reaction than any other approach, so initially we confine our attention to a collinear approach. Two parameters are required to define the nuclear separations: one is the H_A—H_B separation R_{AB}, and the other is the H_B—H_C separation R_{BC}.

At the start of the encounter R_{AB} is infinite and R_{BC} is the H_2 equilibrium bond length. At the end of a successful reactive encounter R_{AB} is equal to the equilibrium bond length and R_{BC} is infinite. The total energy of the three-atom system depends on their relative separations, and can be found by doing a molecular orbital calculation. The plot of the total energy of the system against R_{AB} and R_{BC} gives the potential energy surface of this collinear reaction (Fig. 24.14). This surface is normally depicted as a contour diagram (Fig. 24.15).

When R_{AB} is very large, the variations in potential energy represented by the surface as R_{BC} changes are those of an isolated H_2 molecule as its bond length is altered. A section through the surface at $R_{AB} = \infty$, for example, is the same as the H_2 bonding potential energy curve drawn in Fig. 11.16. At the edge of the diagram where R_{BC} is very large, a section through the surface is the molecular potential energy curve of an isolated H_AH_B molecule.

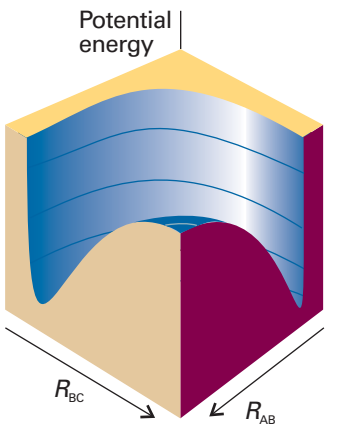

Fig. 24.14 The potential energy surface for the $H + H_2 \rightarrow H_2 + H$ reaction when the atoms are constrained to be collinear.

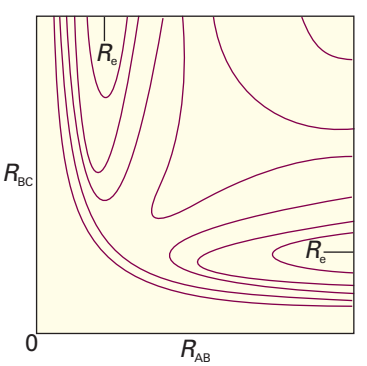

Fig. 24.15 The contour diagram (with contours of equal potential energy) corresponding to the surface in Fig. 24.14. R_e marks the equilibrium bond length of an H_2 molecule (strictly, it relates to the arrangement when the third atom is at infinity).

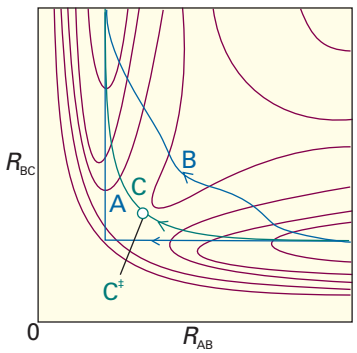

Fig. 24.16 Various trajectories through the potential energy surface shown in Fig. 24.15. Path A corresponds to a route in which R_{BC} is held constant as H_A approaches; path B corresponds to a route in which R_{BC} lengthens at an early stage during the approach of H_A; path C is the route along the floor of the potential valley.

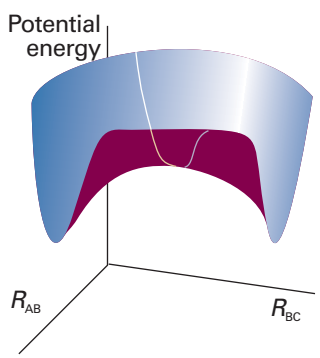

Fig. 24.17 The transition state is a set of configurations (here, marked by the line across the saddle point) through which successful reactive trajectories must pass.

The actual path of the atoms in the course of the encounter depends on their total energy, the sum of their kinetic and potential energies. However, we can obtain an initial idea of the paths available to the system for paths that correspond to least potential energy. For example, consider the changes in potential energy as H_A approaches H_BH_C. If the H_B—H_C bond length is constant during the initial approach of H_A, then the potential energy of the H_3 cluster rises along the path marked A in Fig. 24.16. We see that the potential energy reaches a high value as H_A is pushed into the molecule and then decreases sharply as H_C breaks off and separates to a great distance. An alternative reaction path can be imagined (B) in which the H_B—H_C bond length increases while H_A is still far away. Both paths, although feasible if the molecules have sufficient initial kinetic energy, take the three atoms to regions of high potential energy in the course of the encounter.

The path of least potential energy is the one marked C, corresponding to R_{BC} lengthening as H_A approaches and begins to form a bond with H_B. The H_B—H_C bond relaxes at the demand of the incoming atom, and the potential energy climbs only as far as the saddle-shaped region of the surface, to the **saddle point** marked $C^‡$. The encounter of least potential energy is one in which the atoms take route C up the floor of the valley, through the saddle point, and down the floor of the other valley as H_C recedes and the new H_A—H_B bond achieves its equilibrium length. This path is the reaction coordinate we met in Section 24.4.

We can now make contact with the transition state theory of reaction rates. In terms of trajectories on potential surfaces, the transition state can be identified with a critical geometry such that every trajectory that goes through this geometry goes on to react (Fig. 24.17).

24.8 Some results from experiments and calculations

To travel successfully from reactants to products the incoming molecules must possess enough kinetic energy to be able to climb to the saddle point of the potential surface. Therefore, the shape of the surface can be explored experimentally by changing the relative speed of approach (by selecting the beam velocity) and the degree of vibrational excitation and observing whether reaction occurs and whether the products emerge in a vibrationally excited state (Fig. 24.18). For example, one question that can be answered is whether it is better to smash the reactants together with a lot of translational kinetic energy or to ensure instead that they approach in highly excited vibrational states. Thus, is trajectory $C_2^⋆$, where the H_BH_C molecule is initially vibrationally excited, more efficient at leading to reaction than the trajectory $C_1^⋆$, in which the total energy is the same but has a high translational kinetic energy?

(a) The direction of attack and separation

Figure 24.19 shows the results of a calculation of the potential energy as an H atom approaches an H_2 molecule from different angles, the H_2 bond being allowed to relax to the optimum length in each case. The potential barrier is least for collinear attack, as we assumed earlier. (But we must be aware that other lines of attack are feasible and contribute to the overall rate.) In contrast, Fig. 24.20 shows the potential energy changes that occur as a Cl atom approaches an HI molecule. The lowest barrier occurs for approaches within a cone of half-angle 30° surrounding the H atom. The relevance of this result to the calculation of the steric factor of collision theory should be noted: not every collision is successful, because not every one lies within the reactive cone.

If the collision is sticky, so that when the reactants collide they orbit around each other, the products can be expected to emerge in random directions because all

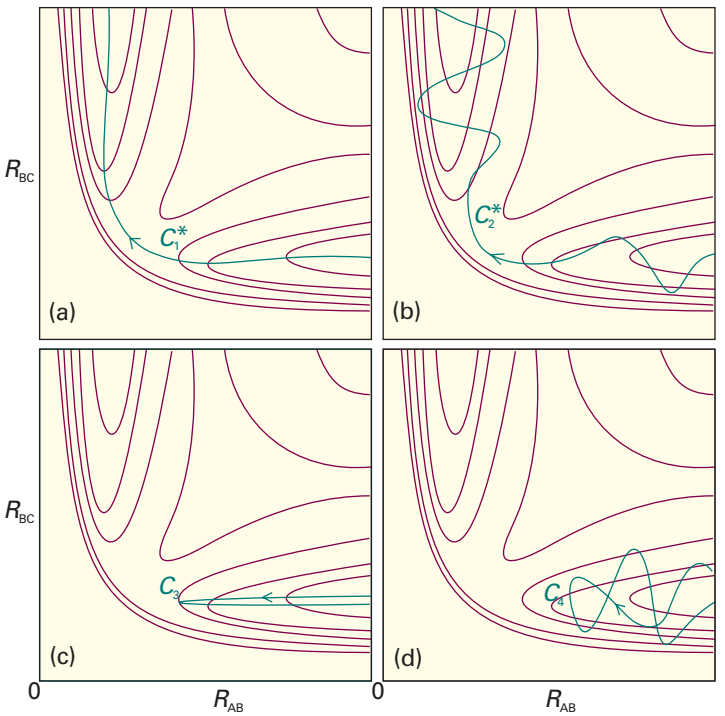

Fig. 24.18 Some successful (*) and unsuccessful encounters. (a) C_1^* corresponds to the path along the foot of the valley. (b) C_2^* corresponds to an approach of A to a vibrating BC molecule, and the formation of a vibrating AB molecule as C departs. (c) C_3 corresponds to A approaching a non-vibrating BC molecule, but with insufficient translational kinetic energy. (d) C_4 corresponds to A approaching a vibrating BC molecule, but still the energy, and the phase of the vibration, is insufficient for reaction.

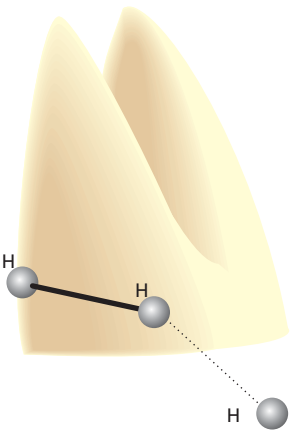

Fig. 24.19 An indication of the anisotropy of the potential energy changes as H approaches H_2 with different angles of attack. The collinear attack has the lowest potential barrier to reaction. The surface indicates the potential energy profile along the reaction coordinate for each configuration.

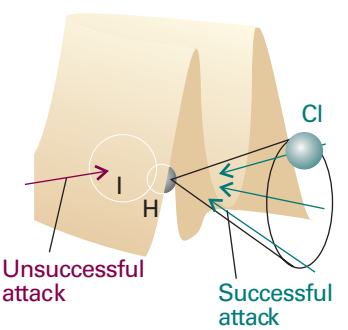

Fig. 24.20 The potential energy barrier for the approach of Cl to HI. In this case, successful encounters occur only when Cl approaches within a cone surrounding the H atom.

memory of the approach direction has been lost. A rotation takes about 1 ps, so if the collision is over in less than that time the complex will not have had time to rotate and the products will be thrown off in a specific direction. In the collision of K and I_2, for example, most of the products are thrown off in the forward direction. This product distribution is consistent with the harpoon mechanism (Section 24.1c) because the transition takes place at long range. In contrast, the collision of K with CH_3I leads to reaction only if the molecules approach each other very closely. In this mechanism, K effectively bumps into a brick wall, and the KI product bounces out in the backward direction. The detection of this anisotropy in the angular distribution of products gives an indication of the distance and orientation of approach needed for reaction, as well as showing that the event is complete in less than 1 ps.

(b) Attractive and repulsive surfaces

Some reactions are very sensitive to whether the energy has been predigested into a vibrational mode or left as the relative translational kinetic energy of the colliding molecules. For example, if two HI molecules are hurled together with more than twice the activation energy of the reaction, then no reaction occurs if all the energy is translational. For F + HCl → Cl + HF, for example, the reaction is about five times as efficient when the HCl is in its first vibrational excited state than when, although HCl has the same total energy, it is in its vibrational ground state.

Comment 24.5

In molecular beam work the remarks we make in our discussion normally refer to directions in a centre-of-mass coordinate system. The origin of the coordinates is the centre of mass of the colliding reactants, and the collision takes place when the molecules are at the origin. The way in which centre-of-mass coordinates are constructed and the events in them interpreted involves too much detail for our present purposes, but we should bear in mind that 'forward' and 'backward' have unconventional meanings. The details are explained in the books in *Further reading*.

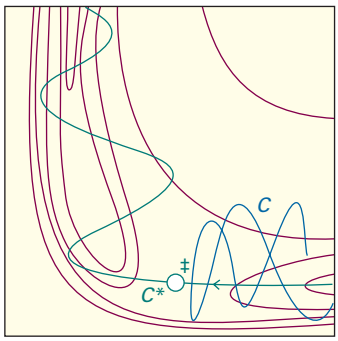

Fig. 24.21 An attractive potential energy surface. A successful encounter (C^*) involves high translational kinetic energy and results in a vibrationally excited product.

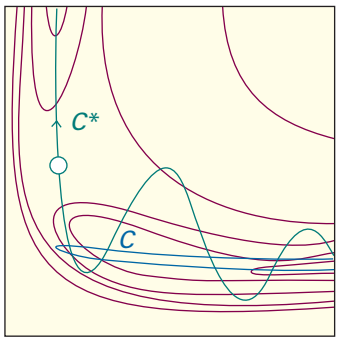

Fig. 24.22 A repulsive potential energy surface. A successful encounter (C^*) involves initial vibrational excitation and the products have high translational kinetic energy. A reaction that is attractive in one direction is repulsive in the reverse direction.

The origin of these requirements can be found by examining the potential energy surface. Figure 24.21 shows an **attractive surface** in which the saddle point occurs early in the reaction coordinate. Figure 24.22 shows a **repulsive surface** in which the saddle point occurs late. A surface that is attractive in one direction is repulsive in the reverse direction.

Consider first the attractive surface. If the original molecule is vibrationally excited, then a collision with an incoming molecule takes the system along *C*. This path is bottled up in the region of the reactants, and does not take the system to the saddle point. If, however, the same amount of energy is present solely as translational kinetic energy, then the system moves along C^* and travels smoothly over the saddle point into products. We can therefore conclude that reactions with attractive potential energy surfaces proceed more efficiently if the energy is in relative translational motion. Moreover, the potential surface shows that once past the saddle point the trajectory runs up the steep wall of the product valley, and then rolls from side to side as it falls to the foot of the valley as the products separate. In other words, the products emerge in a vibrationally excited state.

Now consider the repulsive surface (Fig. 24.22). On trajectory *C* the collisional energy is largely in translation. As the reactants approach, the potential energy rises. Their path takes them up the opposing face of the valley, and they are reflected back into the reactant region. This path corresponds to an unsuccessful encounter, even though the energy is sufficient for reaction. On C^* some of the energy is in the vibration of the reactant molecule and the motion causes the trajectory to weave from side to side up the valley as it approaches the saddle point. This motion may be sufficient to tip the system round the corner to the saddle point and then on to products. In this case, the product molecule is expected to be in an unexcited vibrational state. Reactions with repulsive potential surfaces can therefore be expected to proceed more efficiently if the excess energy is present as vibrations. This is the case with the $H + Cl_2 \rightarrow HCl + Cl$ reaction, for instance.

(c) Classical trajectories

A clear picture of the reaction event can be obtained by using classical mechanics to calculate the trajectories of the atoms taking place in a reaction from a set of initial conditions, such as velocities, relative orientations, and internal energies of the reacting

particles. The initial values used for the internal energy reflect the quantization of electronic, vibrational, and rotational energies in molecules but the features of quantum mechanics are not used explicitly in the calculation of the trajectory.

Figure 24.23 shows the result of such a calculation of the positions of the three atoms in the reaction $H + H_2 \rightarrow H_2 + H$, the horizontal coordinate now being time and the vertical coordinate the separations. This illustration shows clearly the vibration of the original molecule and the approach of the attacking atom. The reaction itself, the switch of partners, takes place very rapidly and is an example of a **direct mode process**. The newly formed molecule shakes, but quickly settles down to steady, harmonic vibration as the expelled atom departs. In contrast, Fig. 24.24 shows an example of a **complex mode process**, in which the activated complex survives for an extended period. The reaction in the illustration is the exchange reaction KCl + NaBr → KBr + NaCl. The tetratomic activated complex survives for about 5 ps, during which time the atoms make about 15 oscillations before dissociating into products.

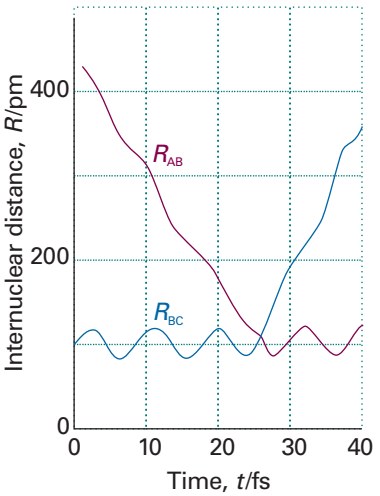

Fig. 24.23 The calculated trajectories for a reactive encounter between A and a vibrating BC molecule leading to the formation of a vibrating AB molecule. This direct-mode reaction is between H and H_2. (M. Karplus, R.N. Porter, and R.D. Sharma, *J. Chem. Phys.*, **43**, 3258 (1965).)

(d) Quantum mechanical scattering theory

Classical trajectory calculations do not recognize the fact that the motion of atoms, electrons, and nuclei is governed by quantum mechanics. The concept of trajectory then fades and is replaced by the unfolding of a wavefunction that represents initially the reactants and finally products.

Complete quantum mechanical calculations of trajectories and rate constants are very onerous because it is necessary to take into account all the allowed electronic, vibrational, and rotational states populated by each atom and molecule in the system at a given temperature. It is common to define a 'channel' as a group of molecules in well-defined quantum mechanically allowed states. Then, at a given temperature, there are many channels that represent the reactants and many channels that represent possible products, with some transitions between channels being allowed but others not allowed. Furthermore, not every transition leads to a chemical reaction. For example, the process $H_2^* + OH \rightarrow H_2 + (OH)^*$, where the asterisk denotes an excited state, amounts to energy transfer between H_2 and OH, whereas the process $H_2^* + OH \rightarrow H_2O + H$ represents a chemical reaction. What complicates a quantum mechanical calculation of trajectories and rate constants even in this simple four-atom system is that many reacting channels present at a given temperature can lead to the desired products $H_2O + H$, which themselves may be formed as many distinct channels. The **cumulative reaction probability**, $N(E)$, at a fixed total energy E is then written as

$$N(E) = \sum_{i,j} P_{ij}(E) \qquad (24.73)$$

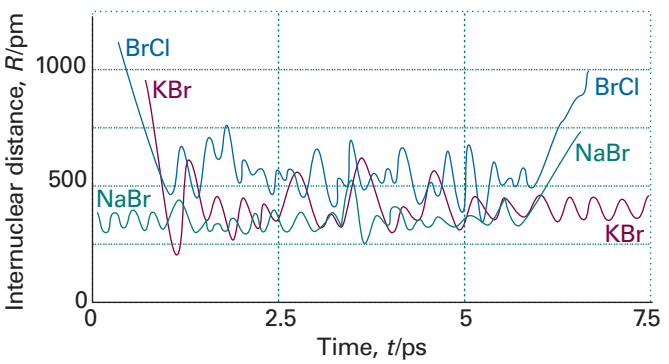

Fig. 24.24 An example of the trajectories calculated for a complex-mode reaction, KCl + NaBr → KBr + NaCl, in which the collision cluster has a long lifetime. (P. Brumer and M. Karplus, *Faraday Disc. Chem. Soc.*, **55**, 80 (1973).)

where $P_{i,j}(E)$ is the probability for a transition between a reacting channel i and a product channel j and the summation is over all possible transitions that lead to product. It is then possible to show that the rate constant is given by

$$k(T) = \frac{\int_0^\infty N(E)\mathrm{e}^{-E/kT}\,\mathrm{d}E}{hQ_\mathrm{r}(T)} \tag{24.74}$$

where $Q_\mathrm{r}(T)$ is the partition function density (the partition function divided by the volume) of the reactants at the temperature T. The significance of eqn 24.74 is that it provides a direct connection between an experimental quantity, the rate constant, and a theoretical quantity, $N(E)$.

24.9 The investigation of reaction dynamics with ultrafast laser techniques

The development of femtosecond pulsed lasers (Section 14.6) has made it possible to make observations on species that have such short lifetimes that in a number of respects they resemble an activated complex. Pulsed-laser techniques can also be used to control the outcome of chemical reactions.

(a) Spectroscopic observation of the activated complex

Until very recently there were no direct spectroscopic observations on activated complexes, for they have a very fleeting existence and often survive for only a few picoseconds. In a typical experiment designed to detect an activated complex, a femtosecond laser pulse is used to excite a molecule to a dissociative state, and then a second femtosecond pulse is fired at an interval after the dissociating pulse. The frequency of the second pulse is set at an absorption of one of the free fragmentation products, so its absorption is a measure of the abundance of the dissociation product. For example, when ICN is dissociated by the first pulse, the emergence of CN from the photoactivated state can be monitored by watching the growth of the free CN absorption (or, more commonly, its laser-induced fluorescence). In this way it has been found that the CN signal remains zero until the fragments have separated by about 600 pm, which takes about 205 fs.

Some sense of the progress that has been made in the study of the intimate mechanism of chemical reactions can be obtained by considering the decay of the ion pair Na^+I^-. As shown in Fig. 24.25, excitation of the ionic species with a femtosecond laser pulse forms an excited state that corresponds to a covalently bonded NaI molecule. The system can be described with two potential energy surfaces, one largely 'ionic' and another 'covalent', which cross at an internuclear separation of 693 pm. A short laser pulse is composed of a wide range of frequencies, which excite many vibrational states of NaI simultaneously. Consequently, the electronically excited complex exists as a superposition of states, or a localized wavepacket (Section 8.6), which oscillates between the 'covalent' and 'ionic' potential energy surfaces, as shown in Fig. 24.25. The complex can also dissociate, shown as movement of the wavepacket toward very long internuclear separation along the dissociative surface. However, not every outward-going swing leads to dissociation because there is a chance that the I atom can be harpooned again, in which case it fails to make good its escape. The dynamics of the system is probed by a second laser pulse with a frequency that corresponds to the absorption frequency of the free Na product or to the frequency at which Na absorbs when it is a part of the complex. The latter frequency depends on the Na···I distance, so an absorption (in practice, a laser-induced fluorescence) is obtained each time the wavepacket returns to that separation.

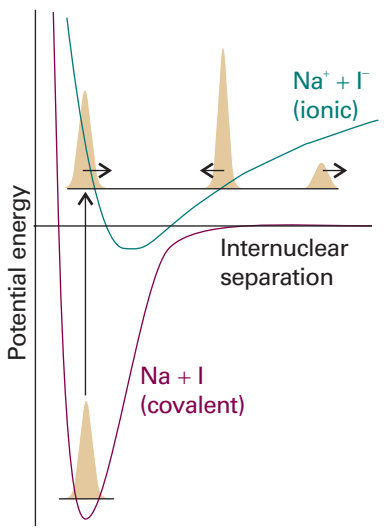

Fig. 24.25 Excitation of the ion pair Na^+I^- forms an excited state with covalent character. Also shown is movement between a 'covalent' surface (in green) and an 'ionic' surface (in purple) of the wavepacket formed by laser excitation.

A typical set of results is shown in Fig. 24.26. The bound Na absorption intensity shows up as a series of pulses that recur in about 1 ps, showing that the wavepacket oscillates with about that period. The decline in intensity shows the rate at which the complex can dissociate as the two atoms swing away from each other. The free Na absorption also grows in an oscillating manner, showing the periodicity of wavepacket oscillation, each swing of which gives it a chance to dissociate. The precise period of the oscillation in NaI is 1.25 ps, corresponding to a vibrational wavenumber of 27 cm^{-1} (recall that the activated complex theory assumes that such a vibration has a very low frequency). The complex survives for about ten oscillations. In contrast, although the oscillation frequency of NaBr is similar, it barely survives one oscillation.

Femtosecond spectroscopy has also been used to examine analogues of the activated complex involved in bimolecular reactions. Thus, a molecular beam can be used to produce a van der Waals molecule (Section 18.6), such as IH···OCO. The HI bond can be dissociated by a femtosecond pulse, and the H atom is ejected towards the O atom of the neighbouring CO_2 molecule to form HOCO. Hence, the van der Waals molecule is a source of a species that resembles the activated complex of the reaction

$$H + CO_2 \rightarrow [HOCO]^{\ddagger} \rightarrow HO + CO$$

The probe pulse is tuned to the OH radical, which enables the evolution of $[HOCO]^{\ddagger}$ to be studied in real time. Femtosecond transition state spectroscopy has also been used to study more complex reactions, such as the Diels–Alder reaction, nucleophilic substitution reactions, and pericyclic addition and cleavage reactions. Biological process that are open to study by femtosecond spectroscopy include the energy-converting processes of photosynthesis and the photostimulated processes of vision. In other experiments, the photoejection of carbon monoxide from myoglobin and the attachment of O_2 to the exposed site have been studied to obtain rate constants for the two processes.

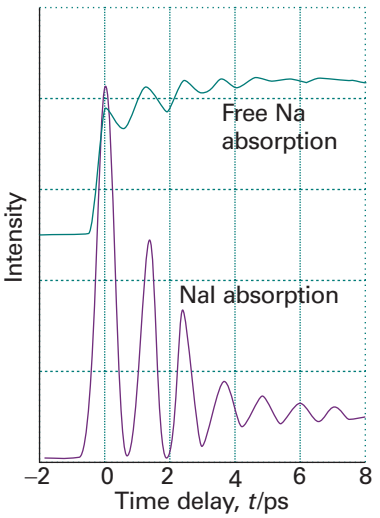

Fig. 24.26 Femtosecond spectroscopic results for the reaction in which sodium iodide separates inot Na and I. The lower curve is the absorption of the electronically excited complex and the upper curve is the absorption of free Na atoms (Adapted from A.H. Zewail, *Science* **242**, 1645 (1988)).

(b) Controlling chemical reactions with lasers

A long-standing goal of chemistry is to control the rate and distribution of products in chemical reactions, with an eye toward minimizing undesirable side reactions and improving the efficiency of industrial processes. We already have at our disposal a number of successful strategies for achieving this goal. For example, it is possible to synthesize a catalyst that accelerates a specific type of reaction but not others, so a desired product may be formed more quickly than an undesired product. However, this strategy is not very general, as a new catalyst needs to be developed for every reaction type of interest. A more ambitious and potentially more powerful strategy consists of using lasers to prepare specific states of reactant molecules that lead to a specific activated complex and hence a specific product, perhaps not even the major product isolated under ordinary laboratory conditions. Here we examine two ways in which the outcome of a chemical reaction can be affected by laser irradiation.

Some reactions may be controlled by exciting the reactants to different vibrational states. Consider the gas-phase reaction between H and HOD. It has been observed that H_2 and OD are the preferred products when thermally equilibrated H atoms react with vibrationally excited HOD molecules prepared by laser irradiation at a wavelength that excites the H—OD stretching mode from the $v = 0$ to the $v = 4$ energy level. On the other hand, when the same stretching mode is excited to the $v = 5$ energy level, HD and OH are the preferred products. This control strategy is commonly referred to as *mode-selective chemistry* and has been used to alter product distributions in a number of bimolecular reactions. However, the technique is limited to those cases in which energy can be deposited and remains localized in the desired vibrational mode of the reactant for a time that is much longer than the reaction time. This is difficult to

achieve in large molecules, in which intramolecular vibrational relaxation redistributes energy among the many vibrational modes within a few picoseconds.

A strategy that seeks to avoid the problem of vibrational relaxation uses ultrafast lasers and is related closely to the techniques used for the spectroscopic detection of transition states. Consider the reaction $I_2 + Xe \rightarrow XeI^* + I$, which occurs via a harpoon mechanism with a transition state denoted as $[Xe^+\cdots I^-\cdots I]$. The reaction can be initiated by exciting I_2 to an electronic state at least 52 460 cm^{-1} above the ground state and then followed by measuring the time dependence of the chemiluminescence of XeI^*. To exert control over the yield of the product, a pair of femtosecond pulses can be used to induce the reaction. The first pulse excites the I_2 molecule to a low energy and unreactive electronic state. We already know that excitation by a femtosecond pulse generates a wavepacket that can be treated as a particle travelling across the potential energy surface. In this case, the wavepacket does not have enough energy to react, but excitation by another laser pulse with the proper wavelength can provide the necessary additional energy. It follows that activated complexes with different geometries can be prepared by varying the time delay between the two pulses, as the partially localized wave packet will be at different locations along the potential energy surface as it evolves after being formed by the first pulse. Because the reaction occurs via the harpoon mechanism, the product yield is expected to be optimal if the second pulse is applied when the wave packet is at a point where the $Xe\cdots I_2$ distance is just right for electron transfer from Xe to I_2 to occur (see Example 24.2). This type of control of the $I_2 + Xe$ reaction has been demonstrated.

So far, the control techniques we have discussed have only been applied to reactions between relatively small molecules, with simple and well-understood potential energy surfaces. Extension of these techniques to the controlled synthesis of materials in routine laboratory work will require much more sophisticated knowledge of how laser pulses may be combined to stimulate a specific molecular response in a complex system.

Electron transfer in homogeneous systems

We end the chapter by applying the concepts of transition state theory and quantum theory to the study of a deceptively simple process, electron transfer between molecules in homogeneous systems. We begin by examining the features of a theory that describes the factors governing the rates of electron transfer. Then, we discuss the theory in the light of experimental results on a variety of systems, including protein complexes. We shall see that relatively simple expressions may be used to predict the rates of electron transfer with reasonable accuracy.

24.10 The rates of electron transfer processes

Consider electron transfer from a donor species D to an acceptor species A in solution. The net reaction is

$$D + A \rightarrow D^+ + A^- \qquad v = k_{obs}[D][A] \qquad K = \frac{[D^+][A^-]}{[D][A]} \tag{24.75}$$

In the first step of the mechanism, D and A must diffuse through the solution and collide to form a complex DA, in which the donor and acceptor are separated by a distance comparable to r, the distance between the edges of each species. We assume that D, A, and DA are in equilibrium:

$$D + A \rightleftharpoons DA \qquad K_{DA} = \frac{k_a}{k'_a} = \frac{[DA]}{[D][A]} \tag{24.76a}$$

where k_a and k'_a are, respectively, the rate constants for the association and dissociation of the DA complex. Next, electron transfer occurs within the DA complex to yield D^+A^-:

$$DA \rightarrow D^+A^- \qquad v_{et} = k_{et}[DA] \tag{24.76b}$$

where k_{et} is the first-order rate constant for the forward electron transfer step. The D^+A^- complex has two possible fates. First, reverse electron transfer with a rate constant k_r can regenerate DA:

$$D^+A^- \rightarrow DA \qquad v_r = k_r[D^+A^-] \tag{24.76c}$$

Second, D^+A^- can break apart and the ions diffuse through the solution:

$$D^+A^- \rightarrow D^+ + A^- \qquad v_d = k_d[D^+A^-] \tag{24.76d}$$

We show in the following *Justification* that

$$\frac{1}{k_{obs}} = \frac{1}{k_a} + \frac{k'_a}{k_a k_{et}}\left(1 + \frac{k_r}{k_d}\right) \tag{24.77}$$

Justification 24.4 *The rate constant for electron transfer in solution*

To find an expression for the second-order rate constant k_{obs} for electron transfer between D and A in solution, we begin by equating the rate of the net reaction (eqn 24.75) to the rate of formation of separated ions, the reaction products (eqn 24.76d):

$$v = k_{obs}[D][A] = k_d[D^+A^-]$$

Now we apply the steady-state approximation to the intermediate D^+A^-:

$$\frac{d[D^+A^-]}{dt} = k_{et}[DA] - k_r[D^+A^-] - k_d[D^+A^-] = 0$$

It follows that

$$[D^+A^-] = \frac{k_{et}}{k_r + k_d}[DA]$$

However, DA is also an intermediate so we apply the steady-state approximation again

$$\frac{d[DA]}{dt} = k_a[D][A] - k'_a[DA] - k_{et}[DA] + k_r[D^+A^-] = 0$$

Substitution of the initial expression for the steady-state concentration of D^+A^- into this expression for [DA] gives, after some algebra, a new expression for $[D^+A^-]$:

$$[D^+A^-] = \frac{k_a k_{et}}{k'_a k_r + k'_a k_d + k_d k_{et}}[D][A]$$

When we multiply this expression by k_d, we see that the resulting equation has the form of the rate of electron transfer, $v = k_{obs}[D][A]$, with k_{obs} given by

$$k_{obs} = \frac{k_d k_a k_{et}}{k'_a k_r + k'_a k_d + k_d k_{et}}$$

To obtain eqn 24.77, we divide the numerator and denominator on the right-hand side of this expression by $k_d k_{et}$ and solve for the reciprocal of k_{obs}.

To gain insight into eqn 24.77 and the factors that determine the rate of electron transfer reactions in solution, we assume that the main decay route for D^+A^- is dissociation of the complex into separated ions, or $k_d \gg k_r$. It follows that

$$\frac{1}{k_{obs}} \approx \frac{1}{k_a}\left(1 + \frac{k'_a}{k_{et}}\right)$$

When $k_{et} \gg k'_a$, we see that $k_{obs} \approx k_a$ and the rate of product formation is controlled by diffusion of D and A in solution, which fosters formation of the DA complex. When $k_{et} \ll k'_a$, we see that $k_{obs} \approx (k_a/k'_a)k_{et}$ or, after using eqn 24.76a,

$$k_{obs} \approx K_{DA}k_{et} \tag{24.78}$$

and the process is controlled by the activation energy of electron transfer in the DA complex. Using transition state theory (Section 24.4), we write

$$k_{et} = \kappa\nu e^{-\Delta^{\ddagger}G/RT} \tag{24.79}$$

where κ is the transmission coefficient, ν is the vibrational frequency with which the activated complex approaches the transition state, and $\Delta^{\ddagger}G$ is the Gibbs energy of activation. Our first task is to write theoretical expressions for $\kappa\nu$ and $\Delta^{\ddagger}G$ by describing the motions of electrons and nuclei mathematically.

24.11 Theory of electron transfer processes

Our discussion concentrates on the following two key aspects of the theory, which was developed independently by R.A. Marcus, N.S. Hush, V.G. Levich, and R.R. Dogonadze:

1 Electrons are transferred by tunnelling through a potential energy barrier, the height of which is partly determined by the ionization energies of the DA and D^+A^- complexes. Electron tunnelling influences the magnitude of $\kappa\nu$.

2 The complex DA and the solvent molecules surrounding it undergo structural rearrangements prior to electron transfer. The energy associated with these rearrangements and the standard reaction Gibbs energy determine $\Delta^{\ddagger}G$.

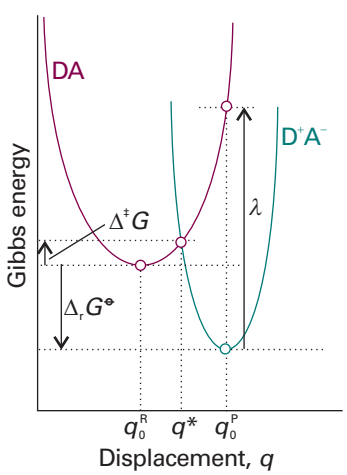

Fig. 24.27 The Gibbs energy surfaces of the complexes DA and D^+A^- involved in an electron transfer process are represented by parabolas characteristic of harmonic oscillators, with the displacement coordinate q corresponding to the changing geometries of the system. In the plot, q_0^R and q_0^P are the values of q at which the minima of the reactant and product parabolas occur, respectively. The parabolas intersect at $q = q^*$. The plots also portray the Gibbs energy of activation, $\Delta^{\ddagger}G$, the standard reaction Gibbs energy, $\Delta_rG^{\ominus}$, and the reorganization energy, λ (discussed in Section 24.11b).

(a) Electron tunnelling

We saw in Section 14.2 that, according to the Franck–Condon principle, electronic transitions are so fast that they can be regarded as taking place in a stationary nuclear framework. This principle also applies to an electron transfer process in which an electron migrates from one energy surface, representing the dependence of the energy of DA on its geometry, to another representing the energy of D^+A^-. We can represent the potential energy (and the Gibbs energy) surfaces of the two complexes (the reactant complex, DA, and the product complex, D^+A^-) by the parabolas characteristic of harmonic oscillators, with the displacement coordinate corresponding to the changing geometries (Fig. 24.27). This coordinate represents a collective mode of the donor, acceptor, and solvent.

According to the Franck–Condon principle, the nuclei do not have time to move when the system passes from the reactant to the product surface as a result of the transfer of an electron. Therefore, electron transfer can occur only after thermal fluctuations bring the geometry of DA to q^* in Fig. 24.27, the value of the nuclear coordinate at which the two parabolas intersect.

The factor $\kappa\nu$ is a measure of the probability that the system will convert from reactants (DA) to products (D^+A^-) at q^* by electron transfer within the thermally excited DA complex. To understand the process, we must turn our attention to the

effect that the rearrangement of nuclear coordinates has on electronic energy levels of DA and D^+A^- for a given distance r between D and A (Fig. 24.28). Initially, the electron to be transferred occupies the HOMO of D, and the overall energy of DA is lower than that of D^+A^- (Fig. 24.28a). As the nuclei rearrange to a configuration represented by q^* in Fig. 24.28b, the highest occupied electronic level of DA and the lowest unoccupied electronic level of D^+A^- become degenerate and electron transfer becomes energetically feasible. Over reasonably short distances r, the main mechanism of electron transfer is tunnelling through the potential energy barrier depicted in Fig. 24.28b. The height of the barrier increases with the ionization energies of the DA and D^+A^- complexes. After an electron moves from the HOMO of D to the LUMO of A, the system relaxes to the configuration represented by q_0^P in Fig. 24.28c. As shown in the illustration, now the energy of D^+A^- is lower than that of DA, reflecting the thermodynamic tendency for A to remain reduced and for D to remain oxidized.

The tunnelling event responsible for electron transfer is similar to that described in Section 9.3, except that in this case the electron tunnels from an electronic level of D, with wavefunction ψ_D, to an electronic level of A, with wavefunction ψ_A. We saw in Section 9.3 that the rate of an electronic transition from a level described by the wavefunction ψ_D to a level described by ψ_A is proportional to the square of the integral

$$\langle H_{DA}\rangle = \int \psi_A \hat{H}_{DA} \psi_B \mathrm{d}\tau$$

where H_{DA} is a hamiltonian that describes the coupling of the electronic wavefunctions. It turns out that in cases where the coupling is relatively weak we may write:

$$\langle H_{DA}\rangle^2 = \langle H_{DA}^\circ\rangle^2 \mathrm{e}^{-\beta r} \qquad (24.80)$$

where r is the edge-to-edge distance between D and A, β is a parameter that measures the sensitivity of the electronic coupling matrix element to distance, and $\langle H_{DA}^\circ\rangle^2$ is the value of the electronic coupling matrix element when D and A are in contact ($r = 0$). The exponential dependence on distance in eqn 24.80 is essentially the same as the exponential decrease in transmission probability through a potential energy barrier described in Section 9.3.

(b) The expression for the rate of electron transfer

The full expression for k_{et} turns out to be (see *Further reading* for a derivation)

$$k_{et} = \frac{2\langle H_{DA}\rangle^2}{h}\left(\frac{\pi^3}{4\lambda RT}\right)^{1/2} \mathrm{e}^{-\Delta^\ddagger G/RT} \qquad (24.81)$$

where $\langle H_{DA}\rangle^2$ can be approximated by eqn 24.80. We show in *Further information* 24.1 that the Gibbs energy of activation $\Delta^\ddagger G$ is

$$\Delta^\ddagger G = \frac{(\Delta_r G^\ominus + \lambda)^2}{4\lambda} \qquad (24.82)$$

where $\Delta_r G^\ominus$ is the standard reaction Gibbs energy for the electron transfer process $DA \rightarrow D^+A^-$, and λ is the **reorganization energy**, the energy change associated with molecular rearrangements that must take place so that DA can take on the equilibrium geometry of D^+A^-. These molecular rearrangements include the relative reorientation of the D and A molecules in DA and the relative reorientation of the solvent molecules surrounding DA. Equation 24.82 shows that $\Delta^\ddagger G = 0$, with the implication that the reaction is not slowed down by an activation barrier, when $\Delta_r G^\ominus = -\lambda$, corresponding to the cancellation of the reorganization energy term by the standard reaction Gibbs energy.

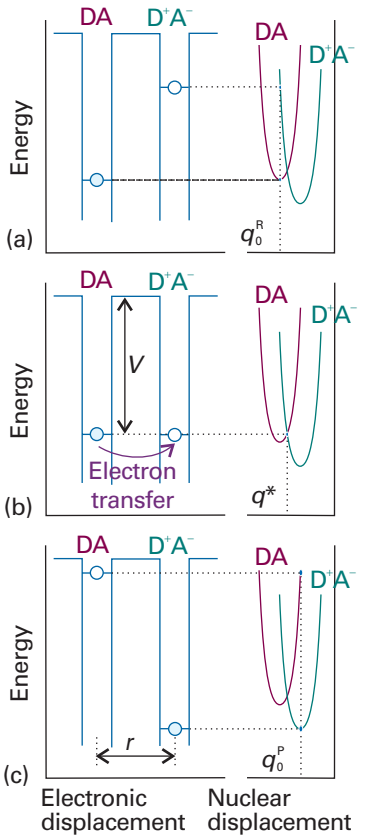

Fig. 24.28 Correspondence between the electronic energy levels (shown on the left) and the nuclear energy levels (shown on the right) for the DA and D^+A^- complexes involved in an electron transfer process. (a) At the nuclear configuration denoted by q_0^R, the electron to be transferred in DA is in an occupied electronic energy level (denoted by a blue circle) and the lowest unoccupied energy level of D^+A^- (denoted by an unfilled circle) is of too high an energy to be a good electron acceptor. (b) As the nuclei rearrange to a configuration represented by q^*, DA and D^+A^- become degenerate and electron transfer occurs by tunnelling through the barrier of height V and width r, the edge-to-edge distance between donor and acceptor. (c) The system relaxes to the equilibrium nuclear configuration of D^+A^- denoted by q_0^P, in which the lowest unoccupied electronic level of DA is higher in energy than the highest occupied electronic level of D^+A^-. (Adapted from R.A. Marcus and N. Sutin, *Biochim. Biophys. Acta* **811**, 265 (1985).)

Equation 24.81 has some limitations. First, it describes only those processes with weak electronic coupling between donor and acceptor. Weak coupling is observed when the electroactive species are sufficiently far apart that the wavefunctions ψ_A and ψ_D do not overlap extensively. An example of a weakly coupled system is the cytochrome *c*–cytochrome b_5 complex, in which the electroactive haem-bound iron ions shuttle between oxidation states +2 and +3 during electron transfer and are about 1.7 nm apart. Strong coupling is observed when the wavefunctions ψ_A and ψ_D overlap very extensively. Examples of strongly coupled systems are mixed-valence, binuclear *d*-metal complexes with the general structure L_mM^{n+}—B—$M^{p+}L_m$, in which the electroactive metal ions are separated by a bridging ligand B. In these systems, $r < 1.0$ nm. The weak coupling limit applies to a large number of electron transfer reactions, including those between proteins during metabolism (*Impact* I7.2). Second, the term $(\pi^3/4\lambda RT)^{1/2}e^{-\Delta^\ddagger G/RT}$ should be used only at high temperatures. At low temperatures, thermal fluctuations alone cannot bring the reactants to the transition state and transition state theory, which is at the heart of the theory presented in this section, fails to account for any observed electron transfer. Electron transfer can still occur, but by *nuclear* tunnelling from the reactant to the product surfaces. We saw in Section 9.5 that the wavefunctions for the lower levels of the quantum mechanical harmonic oscillator extend significantly beyond classically allowed regions, so an oscillator can tunnel into a region of space in which another oscillator may be found. Full quantum mechanical treatments of electron transfer reactions replace the $(\pi^3/4\lambda RT)^{1/2}e^{-\Delta^\ddagger G/RT}$ term with Franck–Condon factors similar to those discussed in Section 14.2, which couple the *nuclear* wavefunctions and provide a measure of the contribution of nuclear tunnelling to the rate of electron transfer.

24.12 Experimental results

It is difficult to measure the distance dependence of k_{et} when the reactants are ions or molecules that are free to move in solution. In such cases, electron transfer occurs after a donor–acceptor complex forms and it is not possible to exert control over *r*, the edge-to-edge distance. The most meaningful experimental tests of the dependence of k_{et} on *r* are those in which the same donor and acceptor are positioned at a variety of distances, perhaps by covalent attachment to molecular linkers (see **1** for an example). Under these conditions, the term $e^{-\Delta^\ddagger G/RT}$ becomes a constant and, after taking the natural logarithm of eqn 24.81 and using eqn 24.80, we obtain

$$\ln k_{et} = -\beta r + \text{constant} \tag{24.83}$$

which implies that a plot of $\ln k_{et}$ against *r* should be a straight line with slope $-\beta$. The value of β depends on the medium through which the electron must travel from donor to acceptor. In a vacuum, $28\ \text{nm}^{-1} < \beta < 35\ \text{nm}^{-1}$, whereas $\beta \approx 9\ \text{nm}^{-1}$ when the intervening medium is a molecular link between donor and acceptor.

The dependence of k_{et} on the standard reaction Gibbs energy has been investigated in systems where the edge-to-edge distance, the reorganization energy, and $\kappa\nu$ are constant for a series of reactions. Then eqn 24.81 becomes

$$\ln k_{et} = -\frac{1}{4\lambda}\left(\frac{\Delta_r G^\ominus}{RT}\right)^2 - \tfrac{1}{2}\left(\frac{\Delta_r G^\ominus}{RT}\right) + \text{constant} \tag{24.84}$$

and a plot of $\ln k_{et}$ (or $\log k_{et}$) against $\Delta_r G^\ominus$ (or $-\Delta_r G^\ominus$) is predicted to be shaped like a downward parabola. Equation 24.84 implies that the rate constant increases as $\Delta_r G^\ominus$ decreases but only up to $-\Delta_r G^\ominus = \lambda$. Beyond that, the reaction enters the **inverted region**, in which the rate constant decreases as the reaction becomes more exergonic ($\Delta_r G^\ominus$ becomes more negative). The inverted region has been observed in a series of

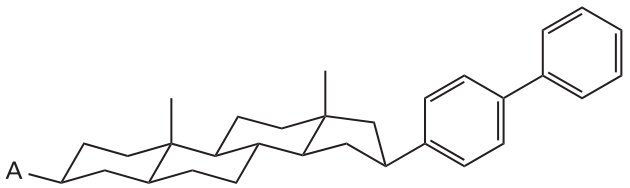

1 An electron donor–acceptor complex

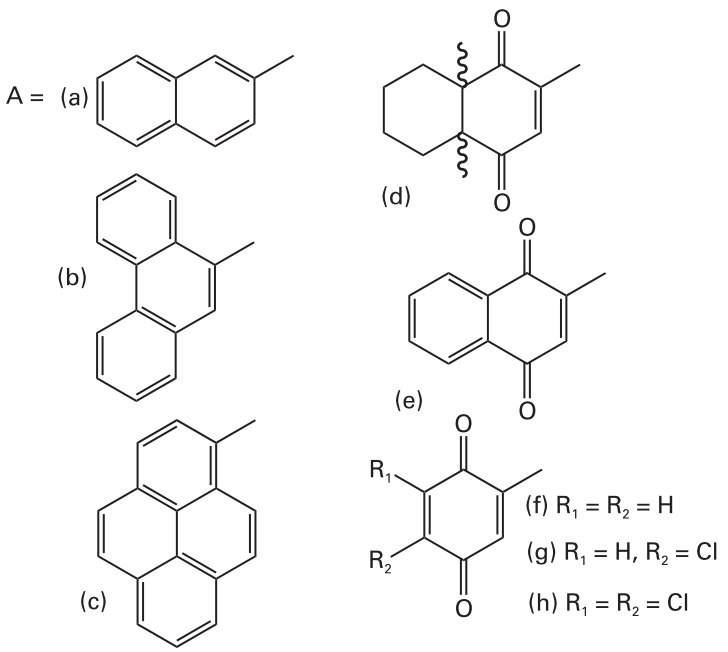

special compounds in which the electron donor and acceptor are linked covalently to a molecular spacer of known and fixed size (Fig. 24.29).

The behaviour predicted by eqn 24.84 and observed experimentally in Fig. 24.29 can be explained by considering the dependence of the activation Gibbs energy on the standard Gibbs energy of electron transfer. We suppose that the energies of the reactant and product complexes can be characterized by parabolas with identical curvatures and fixed but distinct q_0^R and q_0^P. Now we let the minimum energy of the product complex change while keeping q_0^P constant, which corresponds to changing the magnitude of $\Delta_r G^\ominus$. Figure 24.30 shows the effect of increasing the exergonicity of the process. In Fig. 24.30a we see that, for a range of values of $\Delta_r G^\ominus$, $\Delta^\ddagger G > 0$ and the transition state is at $q_a^\star > q_0^R$. As the process becomes more exergonic, the activation Gibbs energy decreases and the rate constant increases. (This behaviour is another example of a 'linear free-energy relation', first discussed in Section 24.5.) Figure 24.30b shows that, when $\Delta^\ddagger G = 0$ and $q_b^\star = q_0^R$, the rate constant for the process reaches a maximum as there is no activation barrier to overcome. According to eqn 24.81, this condition occurs when $-\Delta_r G^\ominus = \lambda$. Finally, Fig. 24.30c shows that, as the process becomes even more exergonic, $\Delta^\ddagger G$ becomes positive again but now the transition state is at $q_c^\star < q_0^R$. The rate constant for the process decreases steadily as the activation barrier for the process increases with decreasing $\Delta_r G^\ominus$. This is the explanation for the 'inverted region' observed in Fig. 24.29.

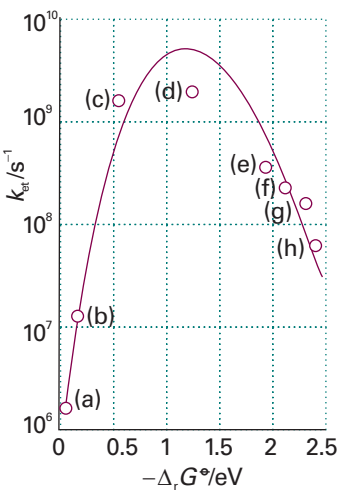

Fig. 24.29 Variation of log k_{et} with $-\Delta_r G^\ominus$ for a series of compounds with the structures given in (**1**). Kinetic measurements were conducted in 2-methyltetrahydrofuran and at 296 K. The distance between donor (the reduced biphenyl group) and the acceptor is constant for all compounds in the series because the molecular linker remains the same. Each acceptor has a characteristic standard reduction potential, so it follows that the standard Gibbs energy for the electron transfer process is different for each compound in the series. The line is a fit to a version of eqn 24.84 and the maximum of the parabola occurs at $-\Delta_r G^\ominus = \lambda = 1.2\ \text{eV} = 1.2 \times 10^2\ \text{kJ mol}^{-1}$. (Reproduced with permission from J.R. Miller, L.T. Calcaterra, and G.L. Closs, *J. Amer. Chem. Soc.* **106**, 3047 (1984).)

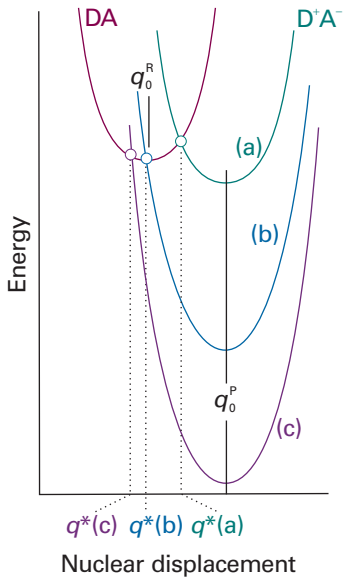

Fig. 24.30 (a) $\Delta^{\ddagger}G > 0$ and the transition state is at $q_a^{\star} > q_0^R$. As the process becomes more exergonic, the activation Gibbs energy decreases and the rate constant increases. (b) When $\Delta^{\ddagger}G = 0$ and $q_b^{\star} = q_0^R$ the rate constant for the process reaches a maximum as there is no activation barrier to overcome. (c) As the process becomes even more exergonic, $\Delta^{\ddagger}G$ becomes positive again but now the transition state is at $q_c^{\star} < q_0^R$. The rate constant for the process decreases steadily as the activation barrier for the process increases with decreasing $\Delta_r G^{\ominus}$.

Some of the key features of electron transfer theory have been tested by experiments, showing in particular the predicted dependence of k_{et} on the standard reaction Gibbs energy and the edge-to-edge distance between electron donor and acceptor. The basic theory presented in Section 24.11 has been extended to transfer of other light particles, such as protons.

IMPACT ON BIOCHEMISTRY

I24.1 Electron transfer in and between proteins

We saw in *Impact* I7.2 and I21.2 that exergonic electron transfer processes drive the synthesis of ATP in the mitochondrion during oxidative phosphorylation. Electron transfer between protein-bound cofactors or between proteins also plays a role in other biological processes, such as photosynthesis (*Impact* I23.2), nitrogen fixation, the reduction of atmospheric N_2 to NH_3 by certain microorganisms, and the mechanisms of action of oxidoreductases, which are enzymes that catalyse redox reactions.

Equation 24.78 applies to a large number of biological systems, such as cytochrome *c* and cytochrome *c* oxidase (*Impact* I7.2), which must form an encounter complex before electron transfer can take place. Electron transfer between protein-bound cofactors can occur at distances of up to about 2.0 nm, a relatively long distance on a molecular scale, with the protein providing an intervening medium between donor and acceptor.

When the electron donor and acceptor are anchored at fixed distances within a single protein, only k_{et} needs to be considered when calculating the rate of electron transfer by using eqn 24.81. Cytochrome *c* oxidase is an example of a system where such intraprotein electron transfer is important. In that enzyme, bound copper ions and haem groups work together to reduce O_2 to water in the final step of respiration. However, there is a great deal of controversy surrounding the interpretation of protein electron transfer data in the light of the theory that leads to eqn 24.81. Much of the available data may be interpreted with $\beta \approx 14\ \text{nm}^{-1}$, a value that appears to be insensitive to the primary and secondary structures of the protein but does depend slightly on the density of atoms in the section of protein that separates donor from acceptor. More detailed work on the specific effect of secondary structure suggests that $12.5\ \text{nm}^{-1} < \beta < 16.0\ \text{nm}^{-1}$ when the intervening medium consists primarily of α helices and $9.0\ \text{nm}^{-1} < \beta < 11.5\ \text{nm}^{-1}$ when the medium is primarily β sheet. Yet another view suggests that the electron takes specific paths through covalent bonds and hydrogen bonds that exist in the protein for the purpose of optimizing the rate of electron transfer.

A value of β is not necessary for the prediction of the rate constants for electron transfer processes between proteins if we take a different approach. It follows from eqns 24.78 and 24.79 that the rate constant k_{obs} may be written as

$$k_{obs} = Ze^{-\Delta^{\ddagger}G/RT} \tag{24.85}$$

where $Z = K_{DA}\kappa\nu$. It is difficult to estimate k_{obs} because we often lack knowledge of β, λ, and $\kappa\nu$. However, when $\lambda \gg |\Delta_r G^{\ominus}|$, k_{obs} may be estimated by a special case of the **Marcus cross-relation**, which we derive in *Further information* 24.1:

$$k_{obs} = (k_{DD}k_{AA}K)^{1/2} \tag{24.86}$$

where K is the equilibrium constant for the net electron transfer reaction (eqn 24.75) and k_{DD} and k_{AA} are the experimental rate constants for the electron self-exchange processes (with the asterisks distinguishing one molecule from another)

$$^*D + D^+ \rightarrow {}^*D^+ + D \tag{24.87a}$$

$$^*A^- + A \rightarrow {}^*A + A^- \tag{24.87b}$$

The rate constants estimated by eqn 24.86 agree fairly well with experimental rate constants for electron transfer between proteins, as we see in the following *Example*.

Example 24.4 *Using the Marcus cross-relation*

The following kinetic and thermodynamic data were obtained for cytochrome *c* and cytochrome c_{551}, two proteins in which haem-bound iron ions shuttle between the oxidation states Fe(II) and Fe(III):

	$k_{ii}/(\text{dm}^3\ \text{mol}^{-1}\ \text{s}^{-1})$	$E^\ominus/\text{V}$
cytochrome *c*	1.5×10^2	0.260
cytochrome c_{551}	4.6×10^7	0.286

Estimate the rate constant k_{obs} for the process

$$\text{cytochrome } c_{551}(\text{red}) + \text{cytochrome } c\,(\text{ox}) \rightarrow \text{cytochrome } c_{551}(\text{ox}) + \text{cytochrome } c(\text{red})$$

Then, compare the estimated value with the observed value of 6.7×10^4 $\text{dm}^3\ \text{mol}^{-1}\ \text{s}^{-1}$.

Method We use the standard potentials and eqns 7.30 ($\ln K = \nu FE^\ominus/RT$) and 7.37 ($E^\ominus = E_R^\ominus - E_L^\ominus$) to calculate the equilibrium constant *K*. Then, we use eqn 24.86, the calculated value of *K*, and the self-exchange rate constants k_{ii} to calculate the rate constant k_{obs}.

Answer The two reduction half-reactions are

$$\text{Right: cytochrome } c\,(\text{ox}) + \text{e}^- \rightarrow \text{cytochrome } c\,(\text{red}) \qquad E_R^\ominus = +0.260\ \text{V}$$
$$\text{Left: cytochrome } c_{551}(\text{ox}) + \text{e}^- \rightarrow \text{cytochrome } c_{551}(\text{red}) \qquad E_L^\ominus = +0.286\ \text{V}$$

The difference is

$$E^\ominus = (0.260\ \text{V}) - (0.286\ \text{V}) = -0.026\ \text{V}$$

It then follows from eqn 7.30 with $\nu = 1$ and $RT/F = 25.69$ mV that

$$\ln K = -\frac{0.026\text{V}}{25.69 \times 10^{-3}\ \text{V}} = -\frac{2.6}{2.569}$$

Therefore, $K = 0.36$. From eqn 24.76 and the self-exchange rate constants, we calculate

$$k_{obs} = \{(1.5 \times 10^2\ \text{dm}^3\ \text{mol}^{-1}\ \text{s}^{-1}) \times (4.6 \times 10^7\ \text{dm}^3\ \text{mol}^{-1}\ \text{s}^{-1}) \times 0.36\}^{1/2}$$
$$= 5.0 \times 10^4\ \text{dm}^3\ \text{mol}^{-1}\ \text{s}^{-1}$$

The calculated and observed values differ by only 25 per cent, indicating that the Marcus relation can lead to reasonable estimates of rate constants for electron transfer.

Self-test 24.4 Estimate k_{obs} for the reduction by cytochrome *c* of plastocyanin, a protein containing a copper ion that shuttles between the +2 and +1 oxidation states and for which $k_{AA} = 6.6 \times 10^2\ \text{dm}^3\ \text{mol}^{-1}\ \text{s}^{-1}$ and $E^\ominus = 0.350$ V.

$[1.8 \times 10^3\ \text{dm}^3\ \text{mol}^{-1}\ \text{s}^{-1}]$

Table 24.3 Summary of uses of k

Symbol	Significance
k	Boltzmann's constant
k_2	Second-order rate constant
k_2°	Rate constant at zero ionic strength
$k_a, k_b, \ldots$	Rate constants for individual steps
$k'_a, k'_b, \ldots$	Rate constants for individual reverse steps
$k^\ddagger$	Rate constant for unimolecular decay of activated complex
K	Equilibrium constant (dimensionless)
K_γ	Ratio of activity coefficients
$K^\ddagger$	Proportionality constant in transition state theory
κ	Transmission coefficient
$\bar{K}$	Equilibrium constant with one mode discarded
k_f	Force constant

Checklist of key ideas

- ☐ 1. In collision theory, it is supposed that the rate is proportional to the collision frequency, a steric factor, and the fraction of collisions that occur with at least the kinetic energy E_a along their lines of centres.
- ☐ 2. A reaction in solution may be diffusion-controlled if its rate is controlled by the rate at which reactant molecules encounter each other in solution. The rate of an activation-controlled reaction is controlled by the rate of accumulating sufficient energy.
- ☐ 3. In transition state theory, it is supposed that an activated complex is in equilibrium with the reactants, and that the rate at which that complex forms products depends on the rate at which it passes through a transition state. The result is the Eyring equation, $k_2 = \kappa(kT/h)\bar{K}_c^\ddagger$.
- ☐ 4. The rate constant may be parametrized in terms of the Gibbs energy, entropy, and enthalpy of activation, $k_2 = (kT/h)e^{\Delta^\ddagger S/R}e^{-\Delta^\ddagger H/RT}$.
- ☐ 5. The kinetic salt effect is the effect of an added inert salt on the rate of a reaction between ions, $\log k_2 = \log k_2^\circ + 2Az_Az_BI^{1/2}$.
- ☐ 6. Techniques for the study of reactive collisions include infrared chemiluminescence, laser-induced fluorescence, multiphoton ionization (MPI), reaction product imaging, and resonant multiphoton ionization (REMPI).
- ☐ 7. A potential energy surface maps the potential energy as a function of the relative positions of all the atoms taking part in a reaction. In an attractive surface, the saddle point (the highest point) occurs early on the reaction coordinate. In a repulsive surface, the saddle point occurs late on the reaction coordinate.
- ☐ 8. Ultrafast laser techniques can be used to probe directly the activated complex and to control the outcome of some chemical reactions.
- ☐ 9. The rate constant of electron transfer in a donor–acceptor complex depends on the distance between electron donor and acceptor, the standard reaction Gibbs energy, and the reorganization energy, λ: $k_{et} \propto e^{-\beta r}e^{-\Delta^\ddagger G/RT}$ (constant T), with $\Delta^\ddagger G = (\Delta_r G^\ominus + \lambda)^2/4\lambda$.
- ☐ 10. The Marcus cross-relation predicts the rate constant for electron transfer in solution from the reaction's equilibrium constant K and the self-exchange rate constants k_{ii}: $k_{obs} = (k_{DD}k_{AA}K)^{1/2}$.

Further reading

Articles and texts

A.J. Alexander and R.N. Zare, Anatomy of elementary chemical reactions. *J. Chem. Educ.* **75**, 1105 (1998).

G.D. Billing and K.V. Mikkelsen, *Advanced molecular dynamics and chemical kinetics*. Wiley, New York (1997).

D.C. Clary, Quantum theory of chemical reaction dynamics. *Science* **279**, 1879 (1998).

F.F. Crim, Vibrational state control of bimolecular reactions: discovering and directing the chemistry. *Acc. Chem. Res.* **32**, 877 (1999).

D.M. Hirst, *Potential energy surfaces*. Taylor and Francis, London (1985).

A.M. Kuznetsov and J. Ulstrup, *Electron transfer in chemistry and biology: an introduction to the theory*. Wiley, New York (1998).

R.D. Levine and R.B. Bernstein, *Molecular reaction dynamics and chemical reactivity*. Clarendon Press, Oxford (1987).

J.I. Steinfeld, J.S. Francisco and W.L. Hase, *Chemical kinetics and dynamics*. Prentice Hall, Upper Saddle River (1999).

A.H. Zewail, Femtochemistry: atomic-scale dynamics of the chemical bond using ultrafast lasers. *Angew. Chem. Int. Ed.* **39**, 2586 (2000).

Further information

Further information 24.1 *The Gibbs energy of activation of electron transfer and the Marcus cross-relation*

The simplest way to derive an expression for the Gibbs energy of activation of electron transfer processes is to construct a model in which the surfaces for DA (the 'reactant complex', denoted R) and for D^+A^- (the 'product complex', denoted P) are described by classical harmonic oscillators with identical reduced masses μ and angular frequencies ω, but displaced minima, as shown in Fig. 24.27. The molar Gibbs energies $G_{m,R}(q)$ and $G_{m,P}(q)$ of the reactant and product complexes, respectively, may be written as

$$G_{m,R}(q) = \tfrac{1}{2}N_A\mu\omega^2(q-q_0^R)^2 + G_{m,R}(q_0^R) \qquad (24.88a)$$

$$G_{m,P}(q) = \tfrac{1}{2}N_A\mu\omega^2(q-q_0^P)^2 + G_{m,P}(q_0^P) \qquad (24.88b)$$

where q_0^R and q_0^P are the values of q at which the minima of the reactant and product parabolas occur, respectively. The standard reaction Gibbs energy for the electron transfer process $DA \rightarrow D^+A^-$ is $\Delta_rG^\ominus = G_{m,P}(q_0^P) - G_{m,R}(q_0^R)$, the difference in standard molar Gibbs energy between the minima of the parabolas. In Fig. 24.27, $\Delta_rG^\ominus < 0$.

We also note that $q^\star$, the value of q corresponding to the transition state of the complex, may be written in terms of the parameter α, the fractional change in q:

$$q^\star = q_0^R + \alpha(q_0^P - q_0^R) \qquad (24.89)$$

We see from Fig. 24.27 that $\Delta^\ddagger G = G_{m,R}(q^\star) - G_{m,R}(q_0^R)$. It then follows from eqns 24.88a, 24.88b, and 24.89 that

$$\Delta^\ddagger G = \tfrac{1}{2}N_A\mu\omega^2(q^\star - q_0^R)^2 = \tfrac{1}{2}N_A\mu\omega^2\{\alpha(q_0^P - q_0^R)\}^2 \qquad (24.90)$$

We now define the reorganization energy, λ, as

$$\lambda = \tfrac{1}{2}N_A\mu\omega^2(q_0^P - q_0^R)^2 \qquad (24.91)$$

which can be interpreted as $G_{m,R}(q_0^P) - G_{m,R}(q_0^R)$ and, consequently, as the (Gibbs) energy required to deform the equilibrium configuration of DA to the equilibrium configuration of D^+A^- (as shown in Fig. 24.27). It follows from eqns 24.90 and 24.91 that

$$\Delta^\ddagger G = \alpha^2\lambda \qquad (24.92)$$

Because $G_{m,R}(q^\star) = G_{m,P}(q^\star)$, it follows from eqns 24.88b, 24.91, and 24.92 that

$$\begin{aligned}\alpha^2\lambda &= \tfrac{1}{2}N_A\mu\omega^2\{(\alpha-1)(q_0^P - q_0^R)\}^2 + \Delta_rG^\ominus \\ &= (\alpha-1)\lambda + \Delta_rG^\ominus\end{aligned} \qquad (24.93)$$

which implies that

$$\alpha = \tfrac{1}{2}\left(\frac{\Delta_rG^\ominus}{\lambda} + 1\right) \qquad (24.94)$$

By combining eqns 24.92 and 24.94, we obtain eqn 24.82. We can obtain an identical relation if we allow the harmonic oscillators to have different angular frequencies and hence different curvatures (see *Further reading*).

Equation 24.82 can be used to derive the form of the Marcus cross-relation (eqn 24.86) used in *Impact* I24.1. We begin by using eqn 24.85 to write the rate constants for the self-exchange reactions as

$$k_{DD} = Z_{DD}e^{-\Delta^\ddagger G_{DD}/RT} \qquad k_{AA} = Z_{AA}e^{-\Delta^\ddagger G_{AA}/RT}$$

For the net reaction (also called the 'cross-reaction') and the self-exchange reactions, the Gibbs energy of activation may be written from eqn 24.82 as

$$\Delta^\ddagger G = \frac{\Delta_rG^{\ominus 2}}{4\lambda} + \frac{\Delta_rG^\ominus}{2} + \frac{\lambda}{4}$$

When $\lambda \gg |\Delta_rG^\ominus|$, we obtain

$$\Delta^\ddagger G = \frac{\Delta_rG^\ominus}{2} + \frac{\lambda}{4}$$

This expression can be used without further elaboration to denote the Gibbs energy of activation of the net reaction. For the self-exchange reactions, we set $\Delta_rG^\ominus_{DD} = \Delta_rG^\ominus_{AA} = 0$ and write

$$\Delta^\ddagger G_{DD} = \frac{\lambda_{DD}}{4} \qquad \Delta^\ddagger G_{AA} = \frac{\lambda_{AA}}{4}$$

It follows that

$$k_{DD} = Z_{DD}e^{-\lambda_{DD}/4RT} \qquad k_{AA} = Z_{AA}e^{-\lambda_{AA}/4RT}$$

To make further progress, we assume that the reorganization energy of the net reaction is the arithmetic mean of the reorganization energies of the self-exchange reactions:

$$\lambda_{DA} = \frac{\lambda_{DD} + \lambda_{AA}}{2}$$

It follows that the Gibbs energy of activation of the net reaction is

$$\Delta^{\ddagger}G = \frac{\Delta_r G^{\ominus}}{2} + \frac{\lambda_{DD}}{8} + \frac{\lambda_{AA}}{8}$$

Therefore, the rate constant for the net reaction is

$$k_{obs} = Ze^{-\Delta_r G^{\ominus}/2RT}e^{-\lambda_{DD}/8RT}e^{-\lambda_{AA}/8RT}$$

We can use eqn 7.17 ($\ln K = -\Delta_r G^{\ominus}/RT$) to write

$$K = e^{-\Delta_r G^{\ominus}/RT}$$

Then, by combining this expression with the expressions for k_{DD} and k_{AA}, and using the relations $e^{x+y} = e^x e^y$ and $e^{x/2} = (e^x)^{1/2}$, we obtain the most general case of the Marcus cross-relation:

$$k_{obs} = (k_{DD}k_{AA}K)^{1/2}f$$

where

$$f = \frac{Z}{(Z_{AA}Z_{DD})^{1/2}}$$

In practice, the factor f is usually set to 1 and we obtain eqn 24.86.

Discussion questions

24.1 Describe the essential features of the harpoon mechanism.

24.2 Distinguish between a diffusion-controlled reaction and an activation-controlled reaction.

24.3 Describe the formulation of the Eyring equation.

24.4 Discuss the physical origin of the kinetic salt effect.

24.5 Describe how the following techniques are used in the study of chemical dynamics: infrared chemiluminescence, laser-induced fluorescence, multiphoton ionization, resonant multiphoton ionization, reaction product imaging, and femtosecond spectroscopy.

24.6 Justify the following statements: (a) Reactions with attractive potential energy surfaces proceed more efficiently if the energy is in relative translational motion. (b) Reactions with repulsive potential surfaces proceed more efficiently if the excess energy is present as vibrations.

24.7 A method for directing the outcome of a chemical reaction consists of using molecular beams to control the relative orientations of reactants during a collision. Consider the reaction $Rb + CH_3I \rightarrow RbI + CH_3$. How should CH_3I molecules and Rb atoms be oriented to maximize the production of RbI?

24.8 Discuss how the following factors determine the rate of electron transfer in homogeneous systems: the distance between electron donor and acceptor, and the reorganization energy of redox active species and the surrounding medium.

Exercises

24.1a Calculate the collision frequency, z, and the collision density, Z, in ammonia, $R = 190$ pm, at 25°C and 100 kPa. What is the percentage increase when the temperature is raised by 10 K at constant volume?

24.1b Calculate the collision frequency, z, and the collision density, Z, in carbon monoxide, $R = 180$ pm at 25°C and 100 kPa. What is the percentage increase when the temperature is raised by 10 K at constant volume?

24.2a Collision theory demands knowing the fraction of molecular collisions having at least the kinetic energy E_a along the line of flight. What is this fraction when (a) $E_a = 10$ kJ mol^{-1}, (b) $E_a = 100$ kJ mol^{-1} at (i) 300 K and (ii) 1000 K?

24.2b Collision theory demands knowing the fraction of molecular collisions having at least the kinetic energy E_a along the line of flight. What is this fraction when (a) $E_a = 15$ kJ mol^{-1}, (b) $E_a = 150$ kJ mol^{-1} at (i) 300 K and (ii) 800 K?

24.3a Calculate the percentage increase in the fractions in Exercise 24.2a when the temperature is raised by 10 K.

24.3b Calculate the percentage increase in the fractions in Exercise 24.2b when the temperature is raised by 10 K.

24.4a Use the collision theory of gas-phase reactions to calculate the theoretical value of the second-order rate constant for the reaction $H_2(g) + I_2(g) \rightarrow 2\,HI(g)$ at 650 K, assuming that it is elementary bimolecular. The collision cross-section is 0.36 nm^2, the reduced mass is 3.32×10^{-27} kg, and the activation energy is 171 kJ mol^{-1}.

24.4b Use the collision theory of gas-phase reactions to calculate the theoretical value of the second-order rate constant for the reaction $D_2(g) + Br_2(g) \rightarrow 2\,DBr(g)$ at 450 K, assuming that it is elementary bimolecular. Take the collision cross-section as 0.30 nm^2, the reduced mass as 3.930 u, and the activation energy as 200 kJ mol^{-1}.

24.5a A typical diffusion coefficient for small molecules in aqueous solution at 25°C is 5×10^{-9} m^2 s^{-1}. If the critical reaction distance is 0.4 nm, what value is expected for the second-order rate constant for a diffusion-controlled reaction?

24.5b Suppose that the typical diffusion coefficient for a reactant in aqueous solution at 25°C is 4.2×10^{-9} m^2 s^{-1}. If the critical reaction distance is 0.50 nm, what value is expected for the second-order rate constant for the diffusion-controlled reaction?

24.6a Calculate the magnitude of the diffusion-controlled rate constant at 298 K for a species in (a) water, (b) pentane. The viscosities are 1.00×10^{-3} kg m^{-1} s^{-1}, and 2.2×10^{-4} kg m^{-1} s^{-1}, respectively.

24.6b Calculate the magnitude of the diffusion-controlled rate constant at 298 K for a species in (a) decylbenzene, (b) concentrated sulfuric acid. The viscosities are 3.36 cP and 27 cP, respectively.

24.7a Calculate the magnitude of the diffusion-controlled rate constant at 298 K for the recombination of two atoms in water, for which $\eta = 0.89$ cP. Assuming the concentration of the reacting species is 1.0 mmol dm^{-3} initially, how long does it take for the concentration of the atoms to fall to half that value? Assume the reaction is elementary.

24.7b Calculate the magnitude of the diffusion-controlled rate constant at 298 K for the recombination of two atoms in benzene, for which $\eta = 0.601$ cP. Assuming the concentration of the reacting species is 1.8 mmol dm^{-3} initially, how long does it take for the concentration of the atoms to fall to half that value? Assume the reaction is elementary.

24.8a For the gaseous reaction A + B → P, the reactive cross-section obtained from the experimental value of the pre-exponential factor is 9.2×10^{-22} m^2. The collision cross-sections of A and B estimated from the transport properties are 0.95 and 0.65 nm^2, respectively. Calculate the P-factor for the reaction.

24.8b For the gaseous reaction A + B → P, the reactive cross-section obtained from the experimental value of the pre-exponential factor is 8.7×10^{-22} m^2. The collision cross-sections of A and B estimated from the transport properties are 0.88 and 0.40 nm^2, respectively. Calculate the *P* factor for the reaction.

24.9a Two neutral species, A and B, with diameters 588 pm and 1650 pm, respectively, undergo the diffusion-controlled reaction A + B → P in a solvent of viscosity 2.37×10^{-3} kg m^{-1} s^{-1} at 40°C. Calculate the initial rate d[P]/dt if the initial concentrations of A and B are 0.150 mol dm^{-3} and 0.330 mol dm^{-3}, respectively.

24.9b Two neutral species, A and B, with diameters 442 pm and 885 pm, respectively, undergo the diffusion-controlled reaction A + B → P in a solvent of viscosity 1.27 cP at 20°C. Calculate the initial rate d[P]/dt if the initial concentrations of A and B are 0.200 mol dm^{-3} and 0.150 mol dm^{-3}, respectively.

24.10a The reaction of propylxanthate ion in acetic acid buffer solutions has the mechanism $A^- + H^+ \rightarrow P$. Near 30°C the rate constant is given by the empirical expression $k_2 = (2.05 \times 10^{13}) e^{-(8681\ K)/T}$ dm^3 mol^{-1} s^{-1}. Evaluate the energy and entropy of activation at 30°C.

24.10b The reaction $A^- + H^+ \rightarrow P$ has a rate constant given by the empirical expression $k_2 = (8.72 \times 10^{12}) e^{-(6134\ K)/T}$ dm^3 mol^{-1} s^{-1}. Evaluate the energy and entropy of activation at 25°C.

24.11a When the reaction in Exercise 24.10a occurs in a dioxane/water mixture that is 30 per cent dioxane by mass, the rate constant fits $k_2 = (7.78 \times 10^{14}) e^{-(9134\ K)/T}$ dm^3 mol^{-1} s^{-1} near 30°C. Calculate $\Delta^{\ddagger}G$ for the reaction at 30°C.

24.11b A rate constant is found to fit the expression $k_2 = (6.45 \times 10^{13}) e^{-(5375\ K)/T}$ dm^3 mol^{-1} s^{-1} near 25°C. Calculate $\Delta^{\ddagger}G$ for the reaction at 25°C.

24.12a The gas-phase association reaction between F_2 and IF_5 is first-order in each of the reactants. The energy of activation for the reaction is 58.6 kJ mol^{-1}. At 65°C the rate constant is 7.84×10^{-3} kPa^{-1} s^{-1}. Calculate the entropy of activation at 65°C.

24.12b A gas-phase recombination reaction is first-order in each of the reactants. The energy of activation for the reaction is 49.6 kJ mol^{-1}. At 55°C the rate constant is 0.23 m^3 s^{-1}. Calculate the entropy of activation at 55°C.

24.13a Calculate the entropy of activation for a collision between two structureless particles at 300 K, taking $M = 50$ g mol^{-1} and $\sigma = 0.40$ nm^2.

24.13b Calculate the entropy of activation for a collision between two structureless particles at 500 K, taking $M = 78$ g mol^{-1} and $\sigma = 0.62$ nm^2.

24.14a The pre-exponential factor for the gas-phase decomposition of ozone at low pressures is 4.6×10^{12} dm^3 mol^{-1} s^{-1} and its activation energy is 10.0 kJ mol^{-1}. What are (a) the entropy of activation, (b) the enthalpy of activation, (c) the Gibbs energy of activation at 298 K?

24.14b The pre-exponential factor for a gas-phase decomposition of ozone at low pressures is 2.3×10^{13} dm^3 mol^{-1} s^{-1} and its activation energy is 30.0 kJ mol^{-1}. What are (a) the entropy of activation, (b) the enthalpy of activation, (c) the Gibbs energy of activation at 298 K?

24.15a The rate constant of the reaction $H_2O_2(aq) + I^-(aq) + H^+(aq) \rightarrow H_2O(l) + HIO(aq)$ is sensitive to the ionic strength of the aqueous solution in which the reaction occurs. At 25°C, $k = 12.2$ dm^6 mol^{-2} min^{-1} at an ionic strength of 0.0525. Use the Debye–Hückel limiting law to estimate the rate constant at zero ionic strength.

24.15b At 25°C, $k = 1.55$ dm^6 mol^{-2} min^{-1} at an ionic strength of 0.0241 for a reaction in which the rate-determining step involves the encounter of two singly charged cations. Use the Debye–Hückel limiting law to estimate the rate constant at zero ionic strength.

24.16a For a pair of electron donor and acceptor, $H_{AB} = 0.03$ cm^{-1}, $\Delta_r G^{\ominus} = -0.182$ eV and $k_{et} = 30.5$ s^{-1} at 298 K. Estimate the value of the reorganization energy.

24.16b For a pair of electron donor and acceptor, $k_{et} = 2.02 \times 10^5$ s^{-1} for $\Delta_r G^{\ominus} = -0.665$ eV. The standard reaction Gibbs energy changes to $\Delta_r G^{\ominus} = -0.975$ eV when a substituent is added to the electron acceptor and the rate constant for electron transfer changes to $k_{et} = 3.33 \times 10^6$ s^{-1}. The experiments were conducted at 298 K. Assuming that the distance between donor and acceptor is the same in both experiments, estimate the values of H_{AB} and λ.

24.17a For a pair of electron donor and acceptor, $k_{et} = 2.02 \times 10^5$ s^{-1} when $r = 1.11$ nm and $k_{et} = 4.51 \times 10^5$ s^{-1} when $r = 1.23$ nm. Assuming that $\Delta_r G^{\ominus}$ and λ are the same in both experiments, estimate the value of β.

24.17b Refer to Exercise 24.17a. Estimate the value of k_{et} when $r = 1.48$ nm.

Problems*

Numerical problems

24.1 In the dimerization of methyl radicals at 25°C, the experimental pre-exponential factor is 2.4×10^{10} dm^3 mol^{-1} s^{-1}. What are (a) the reactive cross-section, (b) the *P* factor for the reaction if the C—H bond length is 154 pm?

24.2 Nitrogen dioxide reacts bimolecularly in the gas phase to give 2 NO + O_2. The temperature dependence of the second-order rate constant for the rate law d[P]/dt = k[NO$_2$]^2 is given below. What are the *P* factor and the reactive cross-section for the reaction?

* Problems denoted with the symbol ‡ were supplied by Charles Trapp, Carmen Giunta, and Marshall Cady.

T/K	600	700	800	1000
k/(cm^3 mol^{-1} s^{-1})	4.6×10^2	9.7×10^3	1.3×10^5	3.1×10^6

Take $\sigma = 0.60$ nm^2.

24.3 The diameter of the methyl radical is about 308 pm. What is the maximum rate constant in the expression $\mathrm{d}[C_2H_6]/\mathrm{d}t = k[CH_3]^2$ for second-order recombination of radicals at room temperature? 10 per cent of a 1.0-dm^3 sample of ethane at 298 K and 100 kPa is dissociated into methyl radicals. What is the minimum time for 90 per cent recombination?

24.4 The rates of thermolysis of a variety of *cis*- and *trans*-azoalkanes have been measured over a range of temperatures in order to settle a controversy concerning the mechanism of the reaction. In ethanol an unstable *cis*-azoalkane decomposed at a rate that was followed by observing the N_2 evolution, and this led to the rate constants listed below (P.S. Engel and D.J. Bishop, *J. Amer. Chem. Soc.* **97**, 6754 (1975)). Calculate the enthalpy, entropy, energy, and Gibbs energy of activation at –20°C.

θ/°C	–24.82	–20.73	–17.02	–13.00	–8.95
$10^4\times k/\mathrm{s}^{-1}$	1.22	2.31	4.39	8.50	14.3

24.5 In an experimental study of a bimolecular reaction in aqueous solution, the second-order rate constant was measured at 25°C and at a variety of ionic strengths and the results are tabulated below. It is known that a singly charged ion is involved in the rate-determining step. What is the charge on the other ion involved?

I	0.0025	0.0037	0.0045	0.0065	0.0085
k/(dm^3 mol^{-1} s^{-1})	1.05	1.12	1.16	1.18	1.26

24.6 The rate constant of the reaction $I^-(aq) + H_2O_2(aq) \rightarrow H_2O(l) + IO^-(aq)$ varies slowly with ionic strength, even though the Debye–Hückel limiting law predicts no effect. Use the following data from 25°C to find the dependence of $\log k_r$ on the ionic strength:

I/(mol kg^{-1})	0.0207	0.0525	0.0925	0.1575
k_r/(dm^3 mol^{-1} min^{-1})	0.663	0.670	0.679	0.694

Evaluate the limiting value of k_r at zero ionic strength. What does the result suggest for the dependence of $\log\gamma$ on ionic strength for a neutral molecule in an electrolyte solution?

24.7 The total cross-sections for reactions between alkali metal atoms and halogen molecules are given in the table below (R.D. Levine and R.B. Bernstein, *Molecular reaction dynamics*, Clarendon Press, Oxford, 72 (1974)). Assess the data in terms of the harpoon mechanism.

σ^*/nm^2	Cl_2	Br_2	I_2
Na	1.24	1.16	0.97
K	1.54	1.51	1.27
Rb	1.90	1.97	1.67
Cs	1.96	2.04	1.95

Electron affinities are approximately 1.3 eV (Cl_2), 1.2 eV (Br_2), and 1.7 eV (I_2), and ionization energies are 5.1 eV (Na), 4.3 eV (K), 4.2 eV (Rb), and 3.9 eV (Cs).

24.8‡ M. Cyfert, B. Latko, and M. Wawrzeczyk (*Int. J. Chem. Kinet.* **28**, 103 (1996)) examined the oxidation of tris(1,10-phenanthroline)iron(II) by periodate in aqueous solution, a reaction that shows autocatalytic behaviour. To assess the kinetic salt effect, they measured rate constants at a variety of concentrations of Na_2SO_4 far in excess of reactant concentrations and reported the following data:

$[Na_2SO_4]$/(mol kg^{-1})	0.2	0.15	0.1	0.05	0.25	0.0125	0.005
k/(dm$^{3/2}$ mol$^{-1/2}$ s^{-1})	0.462	0.430	0.390	0.321	0.283	0.252	0.224

What can be inferred about the charge of the activated complex of the rate-determining step?

24.9‡ For the thermal decomposition of F_2O by the reaction $2\,F_2O(g) \rightarrow 2\,F_2(g) + O_2(g)$, J. Czarnowski and H.J. Schuhmacher (*Chem. Phys. Lett.* **17**, 235 (1972)) have suggested the following mechanism:

(1) $F_2O + F_2O \rightarrow F + OF + F_2O$ k_1
(2) $F + F_2O \rightarrow F_2 + OF$ k_2
(3) $OF + OF \rightarrow O_2 + F + F$ k_3
(4) $F + F + F_2O \rightarrow F_2 + F_2O$ k_4

(a) Using the steady-state approximation, show that this mechanism is consistent with the experimental rate law $-\mathrm{d}[F_2O]/\mathrm{d}t = k[F_2O]^2 + k'[F_2O]^{3/2}$. (b) The experimentally determined Arrhenius parameters in the range 501–583 K are $A = 7.8\times10^{13}$ dm^3 mol^{-1} s^{-1}, $E_a/R = 1.935\times10^4$ K for k and and $A = 2.3\times10^{10}$ dm^3 mol^{-1} s^{-1}, $E_a/R = 1.691\times10^4$ K for k'. At 540 K, $\Delta_fH^\ominus(F_2O) = +24.41$ kJ mol^{-1}, $D(F{-}F) = 160.6$ kJ mol^{-1}, and $D(O{-}O) = 498.2$ kJ mol^{-1}. Estimate the bond dissociation energies of the first and second F—O bonds and the Arrhenius activation energy of reaction 2.

24.10‡ For the gas-phase reaction $A + A \rightarrow A_2$, the experimental rate constant, k_2, has been fitted to the Arrhenius equation with the pre-exponential factor $A = 4.07\times10^5$ dm^3 mol^{-1} s^{-1} at 300 K and an activation energy of 65.43 kJ mol^{-1}. Calculate $\Delta^\ddagger S$, $\Delta^\ddagger H$, $\Delta^\ddagger U$, and $\Delta^\ddagger G$ for the reaction.

24.11‡ One of the most historically significant studies of chemical reaction rates was that by M. Bodenstein (*Z. physik. Chem.* **29**, 295 (1899)) of the gas-phase reaction $2\,HI(g) \rightarrow H_2(g) + I_2(g)$ and its reverse, with rate constants k and k', respectively. The measured rate constants as a function of temperature are

T/K	647	666	683	700	716	781
k/(22.4 dm^3 mol^{-1} min^{-1})	0.230	0.588	1.37	3.10	6.70	105.9
k'/(22.4 dm^3 mol^{-1} min^{-1})	0.0140	0.0379	0.0659	0.172	0.375	3.58

Demonstrate that these data are consistent with the collision theory of bimolecular gas-phase reactions.

24.12 Use the approximate form of the Marcus relation (eqn 24.86 with $f = 1$) to estimate the rate constant for the reaction $Ru(bpy)_3^{3+} + Fe(H_2O)_6^{2+} \rightarrow Ru(bpy)_3^{2+} + Fe(H_2O)_6^{3+}$, where bpy stands for 4,4′-bipyridine. The following data are useful:

$Ru(bpy)_3^{3+} + e^- \rightarrow Ru(bpy)_3^{2+}$ $E^\ominus = 1.26$ V
$Fe(H_2O)_6^{3+} + e^- \rightarrow Fe(H_2O)_6^{2+}$ $E^\ominus = 0.77$ V
$^*Ru(bpy)_3^{3+} + Ru(bpy)_3^{2+} \rightarrow {}^*Ru(bpy)_3^{2+} + Ru(bpy)_3^{3+}$
$k_{Ru} = 4.0\times10^8$ dm^3 mol^{-1} s^{-1}
$^*Fe(H_2O)_6^{3+} + Fe(H_2O)_6^{2+} \rightarrow {}^*Fe(H_2O)_6^{2+} + Fe(H_2O)_6^{3+}$
$k_{Fe} = 4.2$ dm^3 mol^{-1} s^{-1}

Theoretical problems

24.13 Confirm that eqn 24.40 is a solution of eqn 24.39, where $[J]_t$ is a solution of the same equation but with $k = 0$ and for the same initial conditions.

24.14 Evaluate [J]* numerically using mathematical software for integration in eqn 24.40, and explore the effect of increasing reaction rate constant on the spatial distribution of J.

24.15 Estimate the orders of magnitude of the partition functions involved in a rate expression. State the order of magnitude of q_m^T/N_A, q^R, q^V, q^E for typical molecules. Check that in the collision of two structureless molecules the order of magnitude of the pre-exponential factor is of the same order as that predicted by collision theory. Go on to estimate the P factor for a reaction in which $A + B \rightarrow P$, and A and B are nonlinear triatomic molecules.

24.16 Use the Debye–Hückel limiting law to show that changes in ionic strength can affect the rate of reaction catalysed by H^+ from the deprotonation

of a weak acid. Consider the mechanism: $H^+(aq) + B(aq) \rightarrow P$, where H^+ comes from the deprotonation of the weak acid, HA. The weak acid has a fixed concentration. First show that log [H^+], derived from the ionization of HA, depends on the activity coefficients of ions and thus depends on the ionic strength. Then find the relationship between log(rate) and log [H^+] to show that the rate also depends on the ionic strength.

24.17 The Eyring equation can also be applied to physical processes. As an example, consider the rate of diffusion of an atom stuck to the surface of a solid. Suppose that in order to move from one site to another it has to reach the top of the barrier where it can vibrate classically in the vertical direction and in one horizontal direction, but vibration along the other horizontal direction takes it into the neighbouring site. Find an expression for the rate of diffusion, and evaluate it for W atoms on a tungsten surface ($E_a = 60$ kJ mol^{-1}). Suppose that the vibration frequencies at the transition state are (a) the same as, (b) one-half the value for the adsorbed atom. What is the value of the diffusion coefficient D at 500 K? (Take the site separation as 316 pm and $\nu = 1 \times 10^{11}$ Hz.)

24.18 Suppose now that the adsorbed, migrating species treated in Problem 24.17 is a spherical molecule, and that it can rotate classically as well as vibrate at the top of the barrier, but that at the adsorption site itself it can only vibrate. What effect does this have on the diffusion constant? Take the molecule to be methane, for which $B = 5.24$ cm^{-1}.

24.19 Show that the intensities of a molecular beam before and after passing through a chamber of length l containing inert scattering atoms are related by $I = I_0 e^{-\mathcal{N}\sigma l}$, where σ is the collision cross-section and $\mathcal{N}$ the number density of scattering atoms.

24.20 In a molecular beam experiment to measure collision cross-sections it was found that the intensity of a CsCl beam was reduced to 60 per cent of its intensity on passage through CH_2F_2 at 10 μTorr, but that when the target was Ar at the same pressure the intensity was reduced only by 10 per cent. What are the relative cross-sections of the two types of collision? Why is one much larger than the other?

24.21‡ Show that bimolecular reactions between nonlinear molecules are much slower than between atoms even when the activation energies of both reactions are equal. Use transition state theory and make the following assumptions. (1) All vibrational partition functions are close to unity; (2) all rotational partition functions are approximately $1 \times 10^{1.5}$, which is a reasonable order of magnitude number; (3) the translational partition function for each species is 1×10^{26}.

24.22 This exercise gives some familiarity with the difficulties involved in predicting the structure of activated complexes. It also demonstrates the importance of femtosecond spectroscopy to our understanding of chemical dynamics because direct experimental observation of the activated complex removes much of the ambiguity of theoretical predictions. Consider the attack of H on D_2, which is one step in the $H_2 + D_2$ reaction. (a) Suppose that the H approaches D_2 from the side and forms a complex in the form of an isosceles triangle. Take the H—D distance as 30 per cent greater than in H_2 (74 pm) and the D—D distance as 20 per cent greater than in H_2. Let the critical coordinate be the antisymmetric stretching vibration in which one H—D bond stretches as the other shortens. Let all the vibrations be at about 1000 cm^{-1}. Estimate k_2 for this reaction at 400 K using the experimental activation energy of about 35 kJ mol^{-1}. (b) Now change the model of the activated complex in part (a) and make it linear. Use the same estimated molecular bond lengths and vibrational frequencies to calculate k_2 for this choice of model. (c) Clearly, there is much scope for modifying the parameters of the models of the activated complex. Use mathematical software or write and run a program that allows you to vary the structure of the complex and the parameters in a plausible way, and look for a model (or more than one model) that gives a value of k close to the experimental value, 4×10^5 dm^3 mol^{-1} s^{-1}.

Applications: to environmental science and biochemistry

24.23‡ R. Atkinson (*J. Phys. Chem. Ref. Data* **26**, 215 (1997)) has reviewed a large set of rate constants relevant to the atmospheric chemistry of volatile organic compounds. The recommended rate constant for the bimolecular association of O_2 with an alkyl radical R at 298 K is 4.7×10^9 dm^3 mol^{-1} s^{-1} for R = C_2H_5 and 8.4×10^9 dm^3 mol^{-1} s^{-1} for R = cyclohexyl. Assuming no energy barrier, compute the steric factor, P, for each reaction. (*Hint*. Obtain collision diameters from collision cross-sections of similar molecules in the *Data section*.)

24.24‡ The compound α-tocopherol, a form of vitamin E, is a powerful antioxidant that may help to maintain the integrity of biological membranes. R.H. Bisby and A.W. Parker (*J. Amer. Chem. Soc.* **117**, 5664 (1995)) studied the reaction of photochemically excited duroquinone with the antioxidant in ethanol. Once the duroquinone was photochemically excited, a bimolecular reaction took place at a rate described as diffusion-limited. (a) Estimate the rate constant for a diffusion-limited reaction in ethanol. (b) The reported rate constant was 2.77×10^9 dm^3 mol^{-1} s^{-1}; estimate the critical reaction distance if the sum of diffusion constants is 1×10^{-9} m^2 s^{-1}.

24.25 The study of conditions that optimize the association of proteins in solution guides the design of protocols for formation of large crystals that are amenable to analysis by the X-ray diffraction techniques discussed in Chapter 20. It is important to characterize protein dimerization because the process is considered to be the rate-determining step in the growth of crystals of many proteins. Consider the variation with ionic strength of the rate constant of dimerization in aqueous solution of a cationic protein P:

I	0.0100	0.0150	0.0200	0.0250	0.0300	0.0350
$k/k°$	8.10	13.30	20.50	27.80	38.10	52.00

What can be deduced about the charge of P?

24.26 A useful strategy for the study of electron transfer in proteins consists of attaching an electroactive species to the protein's surface and then measuring k_{et} between the attached species and an electroactive protein cofactor. J.W. Winkler and H.B. Gray (*Chem. Rev.* **92**, 369 (1992)) summarize data for cytochrome *c* (*Impact* I7.2) modified by replacement of the haem iron by a zinc ion, resulting in a zinc-porphyrin (ZnP) moiety in the interior of the protein, and by attachment of a ruthenium ion complex to a surface histidine aminoacid. The edge-to-edge distance between the electroactive species was thus fixed at 1.23 nm. A variety of ruthenium ion complexes with different standard reduction potentials were used. For each ruthenium-modified protein, either the $Ru^{2+} \rightarrow ZnP^+$ or the $ZnP^* \rightarrow Ru^{3+}$, in which the electron donor is an electronic excited state of the zinc-porphyrin formed by laser excitation, was monitored. This arrangement leads to different standard reaction Gibbs energies because the redox couples ZnP^+/ZnP and ZnP^+/ZnP^* have different standard potentials, with the electronically excited porphyrin being a more powerful reductant. Use the following data to estimate the reorganization energy for this system:

$-\Delta_r G^\ominus$/eV	0.665	0.705	0.745	0.975	1.015	1.055
$k_{et}/(10^6\ s^{-1})$	0.657	1.52	1.12	8.99	5.76	10.1

24.27 The photosynthetic reaction centre of the purple photosynthetic bacterium *Rhodopseudomonas viridis* contains a number of bound cofactors that participate in electron transfer reactions. The following table shows data compiled by Moser *et al.* (*Nature* **355**, 796 (1992)) on the rate constants for electron transfer between different cofactors and their edge-to-edge distances:

Reaction	$BChl^- \rightarrow BPh$	$BPh^- \rightarrow BChl_2^+$	$BPh^- \rightarrow Q_A$	cyt $c_{559} \rightarrow BChl_2^+$
r/nm	0.48	0.95	0.96	1.23
k_{et}/s^{-1}	1.58×10^{12}	3.98×10^9	1.00×10^9	1.58×10^8

Reaction	$Q_A^- \rightarrow Q_B$	$Q_A^- \rightarrow BChl_2^+$
r/nm	1.35	2.24
k_{et}/s^{-1}	3.98×10^7	63.1

(BChl, bacteriochlorophyll; $BChl_2$, bacteriochlorophyll dimer, functionally distinct from BChl; BPh, bacteriophaeophytin; Q_A and Q_B, quinone molecules bound to two distinct sites; cyt c_{559}, a cytochrome bound to the reaction centre complex). Are these data in agreement with the behaviour predicted by eqn 24.83? If so, evaluate the value of β.

24.28 The rate constant for electron transfer between a cytochrome *c* and the bacteriochlorophyll dimer of the reaction centre of the purple bacterium *Rhodobacter sphaeroides* (Problem 24.27) decreases with decreasing temperature in the range 300 K to 130 K. Below 130 K, the rate constant becomes independent of temperature. Account for these results.

24.29 Azurin is a protein containing a copper ion that shuttles between the +2 and +1 oxidation states, and cytochrome *c* is a protein in which a haem-bound iron ion shuttles between the +3 and +2 oxidation states. The rate constant for electron transfer from reduced azurin to oxidized cytochrome *c* is 1.6×10^3 $dm^3\ mol^{-1}\ s^{-1}$. Estimate the electron self-exchange rate constant for azurin from the following data:

	$k_{ii}/(dm^3\ mol^{-1}\ s^{-1})$	$E^\ominus/V$
cytochrome *c*	1.5×10^2	0.260
azurin	?	0.304